NIST Technical Note 2224

A Simple Correlation for Horizontal Micro-Fin Tube Convective Boiling with Example Calculation

Mark A. Kedzierski
Lingnan Lin

This publication is available free of charge from:
https://doi.org/10.6028/NIST.TN.2224

National Institute of Standards and Technology
U.S. Department of Commerce

NIST Technical Note 2224

A Simple Correlation for Horizontal Micro-Fin Tube Convective Boiling with Example Calculation

Mark A. Kedzierski
Lingnan Lin
Energy and Environment Division
Engineering Laboratory

This publication is available free of charge from:
https://doi.org/10.6028/NIST.TN.2224

June 2022

U.S. Department of Commerce
Gina M. Raimondo , Secretary

National Institute of Standards and Technology
Laurie E. Locasio, Director and Under Secretary of Commerce for Standards and Technology

National Institute of Standards and Technology Technical Note 2224
Natl. Inst. Stand. Technol. Tech. Note 2224, 43 pages (June 2022)
CODEN: NTNOEF

This publication is available free of charge from:
https://doi.org/10.6028/NIST.TN.2224

A Simple Correlation for Horizontal Micro-Fin Tube Convective Boiling with Example Calculation

M. A. Kedzierski and L. Lin
National Institute of Standards and Technology
Gaithersburg, MD 20899

ABSTRACT

This paper presents a simple correlation containing nine dimensionless parameters to predict the local convective boiling heat transfer within a micro-fin tube that was developed from a dataset that included a wide range of refrigerants, flow conditions, and hydraulic diameters. Flow boiling measurements from 36 studies were gathered to produce a dataset containing 29 refrigerants and 15 different hydraulic diameters ranging from 1.8 mm to 6.7 mm. The database was adjusted so that the definition of the Nusselt number, the Reynolds number, the heat flux, and heat transfer coefficient were all defined in the same way for each study. In addition, values for the most recent fluid properties were used for the calculation of dimensionless parameters that were used in the new correlation. The new correlation for micro-fin convective boiling predicted the measurements from the database to within ± 10.3 % for pure-refrigerants and azeotropic mixtures and ± 12.3 % for zeotropic mixtures.

Keywords: boiling, enhanced heat transfer, low-GWP, micro-fin, refrigerant mixtures

TABLE OF CONTENTS

INTRODUCTION[1]

The first micro-fin tube was probably developed around 1938 to solve the problem of dryout in water tube steam boilers (Bailey, 1942). Bailey's patent describes an invention for a tube with 53 internal fins approximately 0.38 mm tall rifling down the tube axis at a helix angle of 60º with the purpose of inducing circumferential flow to maintain the liquid film on the upper portions of the tube wall. Because of the difficulty of mass production in copper, the commercial application of micro-fin tubes to refrigeration and air-conditioning did not occur until the early 1990's (Bogart, 2021). Since its commercial availability, the micro-fin tube has become the most popular internal enhancement for evaporators and condensers of new unitary refrigeration and air-conditioning equipment, primarily as a result of its highest heat transfer with the lowest pressure drop as compared to other enhancements (Webb and Kim, 2005). Consequently, flow boiling heat transfer measurements and prediction models for the micro-fin tube with refrigerants are essential for the evaluation of their use for unitary applications.

As Lin et al. (2022) have shown, despite the fairly long history of the micro-fin tube, a simple and accurate prediction model is still needed. For the last few decades, pressure from the policies set by the Montreal Protocol (1987) and the Kigali Amendment (2016), the Kyoto Protocol (1997) and the European Mobile Directive (2006) have caused a shift to refrigerants with both zero Ozone Depletion Potential (ODP) and low Global Warming Potential (GWP). Consequently, a concerted effort has been made to develop new replacement refrigerants. However, many of the databases that were used to develop popular prediction models contain mainly hydrofluorocarbon (HFC) refrigerants and include only a few of the most recent replacement refrigerants. For example, the Thome et al. (1997) model predicts micro-fin test data for R134a and R123. Cavallini et al. (2006) developed a flow boiling heat transfer model for R22, R134a, R407C, R410A, R507A, and CO_2. Tang and Li (2018) developed a micro-fin flow boiling model using the following seven refrigerants: R22, R134a, R407C, R410A, R1234yf, R1234ze(E), R1234ze(Z) and CO_2. The micro-fin flow boiling correlation by Mehendale (2018) was developed with the following refrigerants: R12, R22, R 32, R134a, R404A, R410A, R1234yf, R1234ze(E), and CO_2. Although extensive, the database used for the Hamilton et al. (2008) model was for the following older refrigerants: R22, R32, R125, R410B, R32/R134a (27/73% and 30/70% mass), and R407C. More recent models from the National Institute of Standards and Technology (NIST) included refrigerants R134a, R1234yf/R134a, and R1234ze(E) (Kedzierski and Park, 2013) and refrigerants R448A, R449A, and R452B (Kedzierski and Kang, 2016). In addition, the databases for correlation development were limited to a single tube diameter for the following models: Thome et al. (1997), Hamilton et al. (2008), Kedzierski and Kang (2016), and Kedzierski and Park (2013). The databases used for the Cavallini et al. (2006), Tang and Li (2018), and Mehendale (2018) correlation had tube diameter of limiting ranges that differed between the studies. Being that the industry is rapidly switching to low-GWP refrigerants, a general model is needed that encompasses most all of the available data for micro-fin tubes so that a wide range of refrigerants and tube diameters can be used to produce an accurate representative predictive model for the HTC of new refrigerants in micro-fin tubes. This endeavor will ensure an accurate

[1]Certain trade names and company products are mentioned in the text or identified in an illustration in order to adequately specify the experimental procedure and equipment used. In no case does such an identification imply recommendation or endorsement by the National Institute of Standards and Technology, nor does it imply that the products are necessarily the best available for the purpose.

sizing of heat transfer equipment for reduced cost and proper performance.

Micro-fin tubes refer to the internally-finned tubes where the fins rifle along the tube axis at a fin-height that is typically shorter than 5 % of the inner tube diameter (Webb and Kim, 2005). Micro-fin tubes can be found with diameters ranging between roughly 2 mm and 12 mm. Recently, the smaller diameter tubes have been made available in order to facilitate compact heat exchanger design and to reduce refrigerant charge. Part of the passive heat transfer enhancement that is associated with micro-fins is the surface area per unit length increase over that of a plain tube, which is between 50 % and 100 %. Other contributions to the heat transfer enhancement include: (1) liquid capillary wicking between the micro-fins, which promotes wetting of the tube circumference and delays dryout (Cavallini et al. (2006) and Thome, 1996); (2) annular flow at lower flow qualities due to the combined effects of swirl flow, as induced by fin rifling, and the capillary effect (Yang and Hrnjak, 2019); (3) reduced nucleate boiling suppression of boiling sites between the fins due to reduced flow velocity between the inner fin region (Thome, 1996). These boiling enhancement mechanisms add significant complexities to the heat transfer process, which is yet to be fully understood.

Recently, Lin et al. (2022) applied the Machine learning (ML) technique to an extensive database that included 7349 flow boiling heat transfer measurements for azeotropic refrigerants within micro-fin tubes. Machine learning, as a branch of artificial intelligence (AI), is a methodology to "learn" the relationships of a set of parameters from data and make predictions without (or with little) explicit instruction. Lin et al. (2022) used this technique to learn what dimensionless parameters were important for modeling the micro-fin flow boiling. The resulting Lin et al. (2022) model consisted of six explicit power law equations where the dimensionless parameters were raised to constant exponents. The Lin et al. (2022) model was able to predict the entire micro-fin heat transfer database to an overall mean absolute error (MAE) of 13.8 %, which is less than any of the previously discussed models. More specifically, the MAEs for the Tang–Li (2018) model and the Mehendale (2018) model against the entire dataset were shown by Lin et al. (2022) to be 20.3 % and 33.9 %, respectively.

Although the Lin et al. (2022) correlation is accurate, it does not model zeotropic mixtures, and it was believed that a simpler, explicit model can be developed. Consequently, the purpose of this paper is to develop a flow boiling heat transfer model for pure and zeotropic refrigerants that is of a simpler form than that of the Lin et al. (2022) model. The modeling form approach for the present analysis is that which was used for the NIST flow boiling models where the dimensionless quantities are raised to functions of quality, rather than being constant. The modeling will use the same data set as was used by Lin et al. (2022) plus zeotropic measurements from the literature. In addition, the present modeling will use the results of the ML approach, which identified the important parameters that govern the micro-fin flow boiling.

DATABASE

An extensive and current database of flow boiling heat transfer coefficients (HTC) for micro-fin tubes has been compiled. This database was developed by Lin et al. (2022) and is extended here to include zeotropic mixtures. The database contains 9859 flow boiling measurements from 36 sources containing 29 refrigerants and 15 different hydraulic diameters ranging from 1.8 mm to 6.7 mm. Tables 1 and 2 summarize the constituent datasets of the database in chronological

order. After removing "outliers" that were statistically identified as having both high influence and high leverage (Belsley et al., 1980), there remained 6001 data points for pure and azeotropic fluids and 1884 data points for zeotropic fluids in the database. The listed publications provided tabulated data and/or plots of the HTC versus vapor quality. Measurements were digitized from figures given in the publications that did not provide tabulated measurements.

The reported measurement uncertainties provided by the various publications were not consistent for the examined database. For example, most works failed to report the confidence level for their uncertainties and whether the uncertainties were estimated from other uncertainties or obtained from repeated measurements. In addition, most researchers provided only an average uncertainty for their entire dataset rather than providing uncertainties for each measurement. This is unfortunate because, ideally, weighting should be used when regressing measurements from different sources to account for differing overall levels of uncertainty. Given that it is not possible to compile a fair comparison of the uncertainties for the literature data due to inconsistencies in their reporting, it was not possible to create a weighting factor that would not potentially introduce a bias to the regression. With this in mind, the measurements for the database were regressed without a weighting factor. Further discussion of the uncertainties of the literature database is provided by Lin et al. (2022).

Table 1 provides a summary of the operating conditions for each study in the database. The database contains only HTC measurements that were obtained from a direct measurement method, i.e., measured wall temperatures at the root of the fin (T_w), saturated refrigerant temperatures (T_s), and heat fluxes (q''). Uncertainties associated with the Wilson (1915) plot, an indirect measurement, rely on both the chosen form of the Wilson (1915) plot and the relative magnitude of the heat transfer resistances, which varies with operating conditions. Accordingly, Wilson (1915) plot HTC uncertainties can be larger and potentially more biased (due to the chosen form of the method, Briggs and Young (1969)) than those associated with direct measure of the HTC. For this reason, measurements that were obtained from the Wilson plot method (e.g., Schlager et al. (1990), Eckels and Pate (1991), and Kuo and Wang, 1996) were excluded from the database. For each citation in the leftmost column, Table 1 shows the range of quality (x_q), heat flux (q''), and refrigerant mass velocity (G_r) for each study in the third through fifth columns. The sixth column provides the approximate saturation temperature or the range for which the data was taken. Although Kedzierski and Kang (2018) and Darabi et al. (1999) argue that a fluid heated boundary condition is more desirable for a flow boiling investigation as it mimics the boundary conditions of applications, the database includes data from both fluid heated and electrically heated tests rigs. This was done to ensure the largest database as possible considering the limited availability of fluid heated tests. Thus, the seventh column of Table 1 identifies the heat boundary condition for each study as either electric or fluid.

Columns 9 through 11 of Table 1 identify how the key governing parameters - heat flux (q''), refrigerant mass velocity (G_r), and HTC ($h_{2\phi}$) - are defined and calculated for each study. As noted by Mehendale (2017), there are considerable inconsistencies in the literature for how the areas are defined for calculating q'', G_r, and $h_{2\phi}$. In Table 1, the symbol Aq in the heading of column nine is used to identify how each citation defined the surface area that was used to

calculate the heat flux. Similarly, the headings for columns ten and eleven are *AG* and *Ah*, respectively. The *AG* identifies the area that was used to calculate the mass velocity. The *Ah* defines the base area for the HTC calculation. Table 1 shows that D_r, D_o, D_t, and D_e have been used to calculate surface areas. The various base areas are defined in the Nomenclature. All of the q'', G_r, and $h_{2\phi}$ measurements associated with those identified in Table 1 were recalculated so that they were based on the actual wetted surface area (A_i), the actual cross sectional flow area (A_{ca}), and the actual surface area (A_i), respectively.

The use of the hydraulic diameter and the actual surface area is to ensure the consistency and relevance of the defined characteristic length and the surface area for all the micro-fin tubes of this study. The actual wetted surface area and the D_h account for variation in the fin parameters, while a nominal area and the root diameter do not. For example, two tubes that have the same root diameter (D_r) but differ in the number and size of the fins would be expected to have different heat transfer performances. Therefore, a correlation based on D_r cannot be expected to capture those performance differences because they have the same characteristic length. It has been well known that turbulent single-phase correlations for a smooth tube can be used to predict other cross-sectional geometries by use of the hydraulic diameter (Kays and Crawford, 1980). The reason for this is that the majority of the heat transfer occurs at the wall. Consequently, the heat transfer is directly linked to the wetted perimeter (the wall). Thus, use of A_i and D_h is an attempt to link the heat transfer physics to something that is proportionally related.

Figure 1 shows the characteristic geometric parameters of a generic micro-fin tube, including the outer diameter D_o, the inner diameter at the fin root D_r, the helix angle α, the apex angle β, the fin height e, and the number of fins n_f. For modeling purposes, a micro-fin is assumed to be an isosceles trapezoid with a fin thickness at the base of t_b and a fin thickness at the tip of t_t. The fin parameters are shown via a cross section perpendicular to the axis of the tube. One of the key efforts of this project was to ensure that all of the HTCs were based on areas and diameters calculated in the same way. All of the measurements that were obtained from the literature were adjusted so that the definition of the Nusselt number, the Reynolds number, the heat flux, and heat transfer coefficient were all defined in the same way for each study. For instance, the surface area for all of the data modeled in this study was ensured to be calculated as the actual inner surface area per unit length (L):

$$\frac{A_i}{L} = 2n_f\sqrt{e^2+\left(\frac{t_b-t_t}{2}\right)^2} + \pi D_r - n_f(t_b-t_t) = 2n_f e\sqrt{1+\tan^2\frac{\beta}{2}} + \pi D_r - 2n_f e\tan\frac{\beta}{2} \qquad (1)$$

Equation (1) is valid for the fin parameters as obtained from a perpendicular (to the tube axis) cross section as shown in Fig. 1. If the fin parameters are given perpendicular to the axis of the micro-fin, which is at a helix angle of α with the tube axis, then the given fin parameters should be used with the eq. (1) and then corrected to obtain the surface area per tube axis length by multiplying the A_i/L as obtained from eq. (1) by $\cos\alpha$.

Figure 2 plots the wetted surface area as calculated by eq. (1) from the fin parameters that were taken from the literature of Tables 1 and 2 versus their respective root diameters. Figure 2 and

the equation $A_i = 5.52D_r$ can be used to approximate the A_i from the known D_r if not all of the parameters required for eq. (1) are known. The dashed lines shown in Fig. 2 are 95 % confidence intervals for the mean A_i, which are, on average, 2.5 mm.

The local heat flux is calculated from the measured heat duty per unit length (q/L) and the actual surface area as:

$$q'' = \frac{q/L}{A_i/L} = \frac{q}{A_i} \tag{2}$$

The convective boiling heat transfer coefficient based on the actual inner surface area ($h_{2\phi}$) is defined as:

$$h_{2\phi} = \frac{q''}{T_w - T_s} \tag{3}$$

The mass velocity and the hydraulic diameter for all of the measurements analyzed in this paper were based on the actual cross sectional flow area (A_{ca}) as calculated from the fin parameters as shown in Fig. 1:

$$A_{ca} = \frac{\pi D_r^2}{4} - \frac{n_f e(t_t + t_b)}{2} = \frac{\pi D_r^2}{4} - n_f e t_b \left(1 - \frac{e t_b}{4 \tan\frac{\beta}{2}}\right) \tag{4}$$

Any mass velocities from the literature that were not based on the A_{ca} were recalculated using eq. (4). In addition, the hydraulic diameter (D_h) was recalculated for all the literature data, if necessary, as:

$$D_h = \frac{\pi D_r^2 - 2n_f e(t_t + t_b)}{2n_f \sqrt{e^2 + \left(\frac{t_b - t_t}{2}\right)^2} + \pi D_r - n_f (t_b - t_t)} = \frac{\pi D_r^2 - 4n_f e t_b \left(1 - \frac{e t_b}{4 \tan\frac{\beta}{2}}\right)}{2n_f \sqrt{e^2 + \left(\frac{e t_b^2}{4 \tan\frac{\beta}{2}}\right)^2} + \pi D_r - n_f \frac{e t_b^2}{2 \tan\frac{\beta}{2}}} \tag{5}$$

The leftmost form of equations (1,4,5) are used when the fin-tip thickness (t_t) is known. The rightmost form of equations (1,4,5) are used when t_t is unknown and β is known.

Figure 2 plots the hydraulic diameters as taken from the literature of Tables 1 and 2 versus their respective root diameters. Figure 2 and the equation $D_h = 0.54D_r$ can be used to approximate the D_h from the known D_r if not all of the parameters required for eq. (5) are known. The dashed lines shown in Fig. 3 are 95 % confidence intervals for the mean D_h, which are, on

average, 0.4 mm.

An estimate of A_{ca} can be obtained from the results of Figs. 1 and 2 and by rearranging the definition of the hydraulic diameter for the flow area as: $A_{ca} = \frac{D_h A_l}{4L} = 0.745 D_r^2$, which is approximately 5 % less than the flow area of a smooth tube with diameter D_r. This implies that that fins, on average, consume 5 % of the flow area of a micro-fin tube as compared to a smooth tube.

Finally, the model developed in this paper is for the local Nusselt number (Nu), which is calculated using the hydraulic diameter and the heat transfer coefficient based on the actual inner surface area of the tube as:

$$\mathrm{Nu} = \frac{h_{2\phi} D_h}{k_l} \tag{6}$$

where k_l is the liquid thermal conductivity of the refrigerant evaluated at the local saturated refrigerant temperature.

MODEL REGRESSION

All of the thermodynamic and transport properties were evaluated with version 10 of REFPROP (Lemmon et al., 2018) and used to calculate the dimensionless numbers for each data point at the local pressure and quality for use in the new correlation. Table 3 shows representative properties for the refrigerants at a saturation temperature of 277.6 K corresponding to those measured in the literature of Tables 1 and 2. Table 4 provides the range of the salient parameters that were used to generate the models and may be taken as the range of validity for the models.

Single Component Refrigerants and Azeotropic Mixtures

The measured local convective boiling Nusselt numbers for the pure-refrigerants and azeotropic mixed refrigerants ($\mathrm{Nu_{pa}}$) were correlated to:

$$\mathrm{Nu_{pa}} = 713.50\,\mathrm{Re}^{C_1}\,\mathrm{Pr}^{C_2}\left(\frac{P_s}{P_c}\right)^{C_3}\mathrm{Bo}^{C_4}\mathrm{Bd}^{C_5}\mathrm{Co}^{C_6}\left(\frac{\rho_l}{\rho_v}\right)^{C_7} \tag{7}$$

where

$$C_1 = 0.53 - 0.64 x_q^2$$
$$C_2 = -0.23 x_q^2$$
$$C_3 = -5.80 x_q + 7.46 x_q^2$$
$$C_4 = 0.44 - 0.77 x_q + 0.40 x_q^2$$

$$C_5 = 0.56 - 0.11x_q$$
$$C_6 = -0.068$$
$$C_7 = -4.70x_q + 6.22x_q^2$$

Here, the all-liquid Reynolds number (Re), the Boiling number (Bo), the liquid Prandtl number (Pr), the reduced pressure (P_s/P_c), the Bond number (Bd), the convection number (Co), and the quality (x_q) are all evaluated locally at the saturation temperature and defined in the Nomenclature. The all-liquid Reynolds number and the Nusselt number are based on the hydraulic diameter (D_h). The Nusselt number is based on the actual inner surface area of the tube (A_i). The absolute percent difference between the measured Nu_p and those predicted by eq. (7) was on average 10.3 %. As shown in Fig. 4, 86.5 % of the measurements are predicted to within ± 20 %. In addition, the predictions are well centered about the mean as illustrated by the average percent difference between the measured and predicted Nu being approximately 1.0 %.

Figure 5 provides an examination of the goodness of the model for the individual pure fluids. The fluids that contribute the greatest number of measurements outside of the 20 % of the mean prediction are CO_2, R22, and R1234ze(E). Of these three fluids, R22 is the largest data set and contributes the greatest number of data points that are either underpredicted or overpredicted by more than 20 %. The R22 data set contains the oldest data of the collective dataset (Lallemand et al., 2001), some of the newest data (Jiang et al., 2016), and two studies in between (Hamilton et al. (2008) and Han et al., 2013a). Two of the R22 studies are heated electrically and two are heated with a fluid. As shown in Table 2, there were five different tubes each with different hydraulic diameters that varied from 4.1 mm to 6.7 mm. Predictions beyond ± 20 % did not correlate with either the heat method or the D_h, nor the age of the study. For example, nearly all of the Hamilton et al. (2008) R22 measurements are predicted to within ± 20 %. Approximately two-thirds of the Han et al. (2013a) R22 data are overpredicted and are shown in Fig. 5 as the cluster of outliers closest to the origin. About 35 % of the Lallemand et al. (2001) R22 measurements are underpredict and are shown as the cluster of data outside the dotted line for the largest Nu. Finally, approximately half of the Jiang et al. (2016) R22 data are underpredicted at the mid Nu range of the R22 plot.

The CO_2 measurements were taken between 2005 and 2010 in four different studies and three different saturation temperature (5 °C, 10 °C and 15 °C), see Table 2. As shown in Fig. 5, the CO_2 datasets for 5 °C and 15 °C remaining within the ± 20 % prediction bounds. Both of the CO_2 datasets for 10 °C have roughly half of their measurements underpredicted by more than 20 % for the higher heat flux measurements and half of the measurements being predicted to within 20 %, which is generally for the lower heat fluxes. Considering that measurement for saturations temperatures of 5 °C and 15 °C are predicted well, it is surmised that the CO_2 outliers have more to do with the higher heat flux condition than the saturation temperature.

Table 2 shows that there were eight different studies between 2012 and 2016 that contributed to the R1234ze(E) data. Similar to the R22 and the CO_2 measurements, no correlation between the various studies and the prediction error was observed. Overall, there is no obvious reason for why CO_2, R22, and R1234ze(E) contribute the most to the number of data outliers. One might suggest a reason being that the probability of measurement variability is greater for datasets

consisting of more contributing studies and ones that are older. However, as shown by Table 2, R134a contains some of the oldest data (2004) and it is made up of 13 different datasets, but yet, it has very few data outside ± 20 % of the prediction.

Figure 6 compares the measured Nu to that predicted by eq. (7) versus quality for representative plots of test runs for nearly fixed Re and P_r. The average Bo is also provided in each figure heading. Symbols are used to represent the measured data, while a solid line provides the prediction. The figures demonstrate the ability of the model to predict various trends with quality, typically within approximately 5 % of the measurement. The Nu for most of the fluids is shown to increase with quality. However, the Nu for CO_2 is shown to slightly decrease with quality and the Nu for R1234ze(E) is shown to be relatively constant.

Zeotropic Mixtures

To predict the flow boiling Nusselt Number for mixtures (Nu_m), a correction factor for eq. (7) was developed. This was done by multiplying the single-component Nusselt Number (Nu_{pa}) by a modifier to predict the Nu for mixtures:

$$Nu_m = Nu_{pa}\left(1 - 0.166\left(\frac{T_d - T_b}{T_b}\right)^{0.12x_q(1-x_q)}\right) \quad (8)$$

where Nu_{pa} is calculated using eq. (7) and T_d and T_b are the dew-point and bubble-point temperatures, respectively, evaluated at the local saturation pressure and overall composition of the mixture. The T_d - T_b difference is commonly called the temperature glide of the mixture. The temperature glide represents the potential for a heat transfer degradation due to mass transfer resistance and loss of available superheat as caused by concentration gradients (Kedzierski et al., 1992). Consequently, the terms in eq. (8) that modify Nu_{pa} describe the mixture degradation effect, which is a function of the normalized temperature glide and quality. A single-component refrigerant would have zero temperature glide that would result in the mixture degradation effect, represented by the bracketed term, being equal to one when $T_d = T_b$. The absolute percent difference between the measured Nu and those predicted by eq. (8) was on average 12.3 %. Figure 7 shows that roughly 80.6 % of the measurements are predicted to within ± 20 %. In addition, the predictions are fairly well centered about the mean because the average precent difference between the measured and the predicted Nu was approximately 7.1 %.

Figure 8 provide an examination of the goodness of the model for the individual zeotropic mixtures. The refrigerant mixtures are shown to be predicted uniformly well with not a large number of measurements being outside the 20 % prediction.

Figure 9 provide representative plots of the Nu for the zeotropic mixture versus quality. The measured Nu is shown as symbols and the Nu as predicted by eq. (8) is given as solid line. As for the plots for the pure fluids and azeotropic mixtures, the plots are for test runs for nearly fixed Re and P_r. The average Bo is also provided in each figure heading. Symbols are used to represent the measured data, while a solid line provides the prediction. The figures demonstrate the ability of the model to predict various trends with quality, typically within approximately

5 % of the measurement. The Nu for most of the fluids is shown to increase with quality. However, the Nu for R515B is shown to slightly decrease with quality and the Nu for R448A is shown to be relatively constant.

EXAMPLE CALCULATION

Calculation of the heat transfer coefficient is required for both the sizing and the rating of a heat exchanger. A rating calculation requires an iterative approach to determine the local heat flux for the calculation of the Bo. For a sizing calculation, the duty of the heat exchanger (q) is known. For electric heating, the heat flux (q''_e) is constant and be calculated from the total tubing length (L), the surface area per unit length as calculated from eq. (1), and the total duty as:

$$q''_e = \frac{q}{(A_i / L)L} \tag{9}$$

A heat flux obtained by fluid heating (q''_f) will vary with the length of tubing and with the direction of the refrigerant flow direction relative to the heat transfer fluid direction. An approximation of the heat flux for pinched counterflow (q''_{fc}) is:

$$q''_{fc} = \frac{2q}{(A_i / L)L}\left(\frac{x_q - x_{qi}}{x_{qo} - x_{qi}}\right) \tag{10}$$

Here, the x_{qi} and the x_{qo} are the entrance and exit qualities, respectively. Similarly, an approximation of the heat flux for pinched parallel flow is:

$$q''_{fp} = \frac{2q}{(A_i / L)L}\left(\frac{x_{qo} - x_q}{x_{qo} - x_{qi}}\right) \tag{11}$$

For multiple flow circuits of unequal length, the heat duty and tube length are associated with each circuit.

The refrigerant mass velocity (G_r) and the Re are based on the actual flow area (A_{ca}) as calculated with eq. (4). The Re is based on D_h and calculated as if the flow were all liquid and independent of quality:

$$\mathrm{Re} = \frac{G_r D_h}{\mu_{r,l}} = \frac{\dot{m}_r D_h}{A_{ca}\mu_{r,l}} \tag{12}$$

where $\dot{m}_r$ is the mass flow rate of the refrigerant. The refrigerant liquid dynamic viscosity ($\mu_{r,l}$) is evaluated at the local equilibrium temperature.

Figure 10 shows an example output of the eq. (7) for a fictitious fluid that can be used to verify the proper implementation of the correlation for three different heating boundary conditions. The heat transfer coefficient was calculated from the Nu while using the D_h and the liquid thermal conductivity as described in eq. (6). The average Bo for the plots is shown

as 0.0001 on the Fig. 10. For counterflow, the Bo varied linearly from near zero at a quality near zero to its maximum value (0.0002) near a quality of 1. Conversely, the Bo for parallel flow varied from 0.0002 to 0 for qualities from near 0 to 1, respectively. The Bo for electric heat was constant at 0.0001 for electric heating.

Figure 10 demonstrates that the convergence of the heat flux for a rating calculation is likely to be stable due to a relatively bounded heat transfer coefficient for wide variation in the heat flux. It is recommended to start an iterative rating calculation with a constant heat flux as calculated from eq. (9). An estimate of the total heat exchanger duty can be used to provide an initial value for the heat flux. The heat flux for the next iteration can be calculated from the heat transfer coefficient from the previous iteration and the measured wall and saturation temperatures:

$$q'' = h_{2\phi}\left(T_w - T_s\right) \tag{13}$$

Relationships Between Various Area Based Parameters

This sub-section provides guidance for converting parameters found in the literature to parameters based on the actual surface area, the actual flow area, and the hydraulic diameter so that they are consistent with the parameters used in the correlation presented in this study. Table 5 provides conversion factors for alternate based mass velocities and Reynolds numbers that can be used to convert to G_r and Re as based on A_{ca} and the D_h. The two-phase Reynolds number is obtained when the all-liquid Reynolds number (Re) is multiplied by the fraction of the mass flow that is liquid, i.e., $1 - x_q$. Consequently, the last column of Table 5 shows $1 - x_q$ in the denominator of the conversion factor for obtaining the all-liquid Reynold number. Table 6 provides conversion factors for obtaining q'', $h_{2\phi}$, and Nu based on A_i and D_h. The conversion factor for the Nu is the same for all alternate based surface areas and alternate diameters as long as the alternate diameter is used to calculate the alternate surface area. Otherwise, a custom conversion factor for the Nu must be derived.

CONCLUSIONS

A new correlation for the local convective boiling Nusselt number for a micro-fin tube for single component and mixed refrigerants was developed from previously published measurements. A large database including 7885 measurements from 36 sources was used. All of the data was converted to being based on the hydraulic diameter and actual surface area for the calculation of the Nusselt number, the heat flux, the heat transfer coefficient, and the Reynolds number. Simple equations are provided to aid the user in the determining the surface area, hydraulic diameter, and the cross-sectional flow area. The following fluids were analyzed here with current fluid properties: CO_2, R22, R32, R125, R134a, R161, R245fa, R1224yd(Z), R1233zd(E), R1234yf, R1234ze(E), R1234ze(Z), R407C, R410A, R410B, R448A, R449A, R450A, R452B, R513A, R515B, R1123/R32 (40/60), R32/R134a (27/73), R32/R134a (30/70), CO_2/R32/R1234ze(E) (9/29/62), R32/R1234ze(E) (20/80), R32/R1234ze(E) (30/70), R32/R1234ze(E) (40/60), and R32/R1234ze(E) (50/50). The new correlation predicted the measurements to within ± 10.3 % for pure refrigerants and azeotropic mixtures and ± 12.3 % for zeotropic mixtures. The correlation is valid for a wide range of hydraulic diameters and operating conditions while using only nine dimensionless parameters.

In general, the measured boiling heat-transfer coefficient increased with increasing. However, this was not always the case for all refrigerants, e.g., CO_2. Mixed refrigerants were predicted by multiplying the pure refrigerant correlation with a term containing the dimensionless temperature glide, which was designed to reduce to 1 for zero glides.

ACKNOWLEDGEMENTS

This work was funded by NIST. The authors thank the following for their constructive criticism of the first draft of the manuscript: P. Domanski from NIST, and Ki-Jung Park from the Korea Atomic Energy Research Institute.

NOMENCLATURE

English symbols

A_{ca} actual cross-sectional flow area, eq. (4) (m^2)

A_{cm} cross-sectional flow area of an equivalent smooth tube of diameter of D_m, $(\pi D_m^2)/4$ (m^2)

A_{co} cross-sectional flow area of an equivalent smooth tube of diameter of D_o, $(\pi D_o^2)/4$ (m^2)

A_{cr} cross-sectional flow area of smooth tube of diameter of D_r, $(\pi D_r^2)/4$ (m^2)

A_{ct} cross-sectional flow area of smooth tube of diameter of D_t, $(\pi D_t^2)/4$ (m^2)

A_e inner surface area of an equivalent smooth tube with the diameter of D_e, $\pi D_e L$ (m^2)

AG symbol use in Table 1 to denote area used to calculate mass velocity (-)

Ah symbol use in Table 1 to denote area used to calculate HTC (-)

A_i actual inner surface area, eq. (1) (m^2)

A_m inner surface area of an equivalent smooth tube of diameter of D_m, $\pi D_m L$ (m^2)

Aq symbol use in Table 1 to denote area used to calculate heat flux (-)

A_r inner surface area of an equivalent smooth tube of diameter of D_r, $\pi D_r L$ (m^2)

A_t inner surface area of an equivalent smooth tube of diameter of D_t, $\pi D_t L$ (m^2)

Bd Bond number, $\dfrac{gD_h(\rho_l-\rho_v)e}{\sigma n_f}$

Bo local boiling number, $\dfrac{q''}{G_r i_{fg}}$

C subscripted coefficients given in eqs. (4) and (5) for exponents

Co convection number, $\left(\dfrac{1-x_q}{x_q}\right)^{0.8}\left(\dfrac{\rho_v}{\rho_l}\right)^{0.5}$

c_p specific heat (J kg^{-1} K^{-1})

D_e equivalent inner diameter of smooth tube, $D_e=\sqrt{\dfrac{4A_{ca}}{\pi}}$ (m)

D_h hydraulic diameter of micro-fin tube defined in eq. (5) (m)

D_o outer diameter, $D_r + 2t_w$ (m)

D_t inner diameter at the fin tip, $D_o - 2e - 2t_w$ (m)

D_r inner diameter at the fin root, $D_o - 2t_w$ (m)

D_m mean inner diameter, $(D_o + D_r)/2$ (m)

e fin height (m)

g acceleration due to gravity (m s^{-2})

G_r total refrigerant mass velocity based on A_{ca}, $G_r=\dfrac{\dot{m}_r}{A_{ca}}$ (kg m^{-2} s^{-1})

$h_{2\phi}$ local two-phase heat-transfer coefficient (W $m^{-2}\cdot K^{-1}$)

i_{fg} latent heat of vaporization (J kg^{-1})

k refrigerant thermal conductivity (W m^{-1} K^{-1})

L length of tube (m)

$\dot{m}_r$ mass flow rate of refrigerant (kg s^{-1})

n_f number of micro-fins (-)

Nu local Nusselt number based on D_h and defined in eq. (6) (-)

P local fluid pressure (Pa)

P_r local reduced fluid pressure, P/P_c (-)

Pr liquid refrigerant Prandtl number $\left.\frac{c_p \mu}{k}\right|_{r,l}$

q heat duty (W)

q" local heat flux based on A_i (W m^{-2})

Re all liquid, refrigerant Reynolds number based on D_h , $\mathrm{Re} = \frac{G_r D_h}{\mu_{r,l}}$

s distance between fins (m)

T temperature (K)

T_w wall temperature evaluated the root of the fin (K)

t_b thickness of base of micro-fin (m)

t_t thickness of tip of micro-fin (m)

t_w tube wall thickness (m)

x_q thermodynamic mass quality (-)

Greek symbols

α helix angle of fin with respect to tube axis defined in Fig. 1 (°)

β fin apex angle defined in Fig. 1 (°)

ΔT_s T_s - T_w (K)

μ viscosity (Pa·s)

ρ density (kg m^{-3})

σ surface tension (kg s^{-2})

Subscripts

b bubble point

c critical condition

d dew point

e exit, electric

f fluid

i inlet

l liquid

m mixture

p prediction

pa pure and azeotropic refrigerants

r refrigerant

s saturated state

v vapor

w heat transfer surface

REFERENCES

Baba D, Nakagawa T, Koyama S. 2012. Flow Boiling Heat Transfer and Pressure Drop of R1234ze(E) and R32 in a Horizontal Micro-Fin Tube. *Int. Refrig. Air Cond. Conf.*, p. Paper 1218. https://doi.org/10.18462/iir.tptpr.2017.0078.

Bailey, E. G. 1942. Liquid Vaporizing Tube, US patent 2,279,548. https://patents.google.com/patent/US2279548A/en

Bandarra Filho EP, Jabardo JMS. 2006. Convective boiling performance of refrigerant R-134a in herringbone and microfin copper tubes. Int J Refrig;29:81–91. https://doi.org/10.1016/j.ijrefrig.2005.05.011.

Bandarra Filho EP, Barbieri PEL. 2011. Flow boiling performance in horizontal microfinned copper tubes with the same geometric characteristics. Exp Therm Fluid Sci;35:832–40. https://doi.org/10.1016/j.expthermflusci.2010.06.012.

Belsley, D. A., Kuh, E., and Welsch, R. E. 1980. Regression Diagnostics: Identifying Influential Data and Sources of Collinearity, New York: Wiley.

Bogart, J. 2021. Private Communications. York International, York, PA.

Briggs, D. E., and Young, E.H. 1969. Modified Wilson Plot Techniques for Obtaining Heat Transfer Correlations for Shell and Tube Heat Exchangers, *Chem. Engr. Progr. Symp. Ser. No. 92*, 65, 35-45.

Cavallini A, Col D Del, Rossetto L, Tecnica F, and Padova U. 2006. Flow boiling inside microfin tubes: prediction of the heat transfer coefficient. ECI Int. Conf. Boil. Heat Transf., Spoleto, Italy.

Dang C, Haraguchi N, Hihara E. 2010. Flow boiling heat transfer of carbon dioxide inside a small-sized microfin tube. Int J Refrig;33:655–63. https://doi.org/10.1016/j.ijrefrig.2010.01.003.

Diani A, Cavallini A, Rossetto L. 2017. R1234yf Flow Boiling Heat Transfer Inside a 2.4-mm Microfin Tube. Heat Transf Eng;38:303–12. https://doi.org/10.1080/01457632.2016.1189260.

Diani A, Mancin S, Cavallini A, Rossetto L. 2016. Experimental investigation of R1234ze(E) flow boiling inside a 2.4 mm ID horizontal microfin tube. Int J Refrig;69:272–84. https://doi.org/10.1016/j.ijrefrig.2016.06.014.

Diani A, Mancin S, Rossetto L. 2014. R1234ze(E) flow boiling inside a 3.4 mm ID microfin tube. Int J Refrig;47:105–19. https://doi.org/10.1016/j.ijrefrig.2014.07.018.

Diani A, Mancin S, Rossetto L. 2015. Flow boiling heat transfer of R1234yf inside a 3.4mm ID microfin tube. Exp Therm Fluid Sci;66:127–36. https://doi.org/10.1016/j.expthermflusci.2015.03.019.

Diani A, and Rossetto L. 2019. R513A flow boiling heat transfer inside horizontal smooth tube and microfin tube. Int J Refrig;107:301–14. https://doi.org/10.1016/j.ijrefrig.2019.07.023.

Diani A, and Rossetto L. 2018. Experimental analysis of refrigerants flow boiling inside small sized microfin tubes. Heat Mass Transf Und Stoffuebertragung;54:2315–29. https://doi.org/10.1007/s00231-017-2111-7.

Diani A, and Rossetto L. 2015. Vaporization inside a mini microfin tube: experimental results and modeling. J Phys Conf Ser;655:012032. https://doi.org/10.1088/1742-6596/655/1/012032.

Darabi, J.D., Ohadi, M.M., Fanni, M.A., Dessiatoun, S.V., and Kedzierski, M.A. 1999. Effect of
Heating Boundary Conditions on Pool Boiling Experiments, HVAC&R Research, 5(4), 283-296.

Directive 2006/40/EC of The European Parliament & of the Council of 17 May 2006 Relating to Emissions from Air-Conditioning Systems in Motor Vehicles & Amending Council Directive 70/156/EC. Official Journal of the European Union, 49(L 161):12-18. https://www.legislation.gov.uk/eudr/2006/40/adopted/data.pdf

Eckels, S. J., Pate, M. B. 1991. Evaporation and Condensation of HFC-134a and CFC-12 in a Smooth Tube and a Micro-Fin Tube (RP-630). ASHRAE Trans, 97:68–78.

Gao L, Honda T, Koyama S. 2007. Experiments on flow boiling heat transfer of almost pure CO2 and CO2-Oil Mixtures in Horizontal Smooth and Microfin Tubes. HVAC R Res;13:415–25. https://doi.org/10.1080/10789669.2007.10390962.

Hamilton, L. J., Kedzierski, M. A, and Kaul, M. P. 2008. Horizontal convective boiling of pure and mixed refrigerants within a micro-fin tube. *Journal of Enhanced Heat Transfer* 15(3):211-226. https://doi.org/10.1615/JEnhHeatTransf.v15.i3.30

Han X, Li P, Wang Z, Wang X, Zhang X, Chen G. 2013a. Evaporation heat transfer and pressure drop of R161 in a 7mm micro-fin tube. Int J Heat Mass Transf;62:638–46. https://doi.org/10.1016/j.ijheatmasstransfer.2013.03.017.

Han X, Li P, Yuan X, Wang Q, Chen G. 2013b. The boiling heat transfer characteristics of the mixture HFO-1234yf/oil inside a micro-fin tube. Int J Heat Mass Transf;67:1122–30. https://doi.org/10.1016/j.ijheatmasstransfer.2013.08.083.

Hu, H., Ding, G., Wang, K. 2008. Heat transfer characteristics of R410A-oil mixture flow boiling inside a 7 mm straight microfin tube. Int. J. Refrig. 31, 1081–1093. https://doi.org/10.1016/j.ijrefrig.2007.12.004

Jiang GB, Tan JT, Nian QX, Tang SC, Tao WQ. 2016. Experimental study of boiling heat transfer in smooth/micro-fin tubes of four refrigerants. Int J Heat Mass Transf;98:631–42. https://doi.org/10.1016/j.ijheatmasstransfer.2016.03.024.

Kays, W. M., and Crawford, M. E. 1980 Convective Heat and Mass Transfer, McGraw-Hill, New York, NY

Kedzierski, M. A., and Lin, L. 2021. Update of Legacy NIST Horizontal Micro-Fin Tube Convective Boiling Measurements and Model with Current Fluid Property Values, NIST Technical Note 2179, U.S. Department of Commerce, Washington, D.C.

Kedzierski, M. A., Kang, D, 2018 Horizontal Convective Boiling of R1234yf, R134a, and R450A within a Micro-Fin Tube, International Journal of Refrigeration, doi:10.1016/j.ijrefrig.2018.02.021

Kedzierski, M. A., and Kang, D. Y. 2016. Horizontal convective boiling of R448A, R449A, and R452B within a micro-fin tube, *Science and Technology for the Built Environment* 22:8, 1090-1103.

Kedzierski, M. A., and Park, K. J. 2013. Horizontal convective boiling of R134a, R1234yf/R134a, and R1234ze(E) within a micro-fin tube. *J. of Enhanced Heat Transfer*. 20(4): 333-346.

Kedzierski, M. A., Kim, J. H., and Didion, D. A. 1992. Causes of the apparent heat transfer degradation for refrigerant mixtures. *Two-Phase Flow and Heat Transfer, HTD-Vol. 197*, J. H. Kim, R. A. Nelson, and A. Hashemi, Eds., ASME, New York, 197:149-158.

Kigali Amendment. 2106. *Amendment to the Montreal Protocol on Substances that Deplete the Ozone Layer*. United Nations (UN), New York, NY, USA.

Kondou, C., .2019. Heat transfer and pressure drop of R1123/R32 (40/60 mass%) flow in horizontal microfin tubes during condensation and evaporation. Sci. Technol. Built Environ. 25, 1281–1291. https://doi.org/10.1080/23744731.2019.1642096

Kondou C, Baba D, Mishima F, Koyama S. 2013. Flow boiling of non-azeotropic mixture R32/R1234ze(E) in horizontal microfin tubes. Int J Refrig;36:2366–78. https://doi.org/10.1016/j.ijrefrig.2013.07.009.

Kondou C, Mishima F, Liu J, Koyama S. 2014a. Condensation and Evaporation of R134a , R1234ze (E) and R1234ze (Z) Flow in Horizontal Microfin Tubes at Higher Temperature. *Int Refrig Air Cond Conf.*

Kondou C, Mishima F, Liu J, Koyama S. 2014b. Condensation and Evaporation of R744/R32/R1234ze(E) Flow in Horizontal Microfin Tubes. *Int. Refrig. Air Cond. Conf.*, Paper 1448.

Kuo, C.S., Wang, C.C. 1996. In-tube evaporation of HCFC-22 in a 9.52 mm micro-fin/smooth tube. Int J Heat Mass Transf, 39:2559–69. https://doi.org/10.1016/0017-9310(95)00326-6.

Kyoto Protocol 1997. *United Nations Framework Convention on Climate Change.* United Nations (UN), New York, NY, USA.

Lallemand M, Branescu C, Haberschill P. 2001. Local heat transfer coeffcients during boiling of R22 and R407C in horizontal smooth and microfin tubes. Int J Refrig;24:57–72. https://doi.org/10.1016/S0140-7007(00)00064-5.

Lemmon, E. W., Huber, M. L., and McLinden, M. O. 2018. *NIST Standard Reference Database 23 (REFPROP), Version 10*. Private Communications with McLinden, National Institute of Standards and Technology, Boulder, CO.

Lin, L., Gao, L., Kedzierski, M. A., and Hwang, Y. 2022. A general model for flow boiling heat transfer in microfin tubes based on a new neural network architecture, Energy AI, 8, 100151.

Longo GA, Mancin S, Righetti G, Zilio C. 2017a. R245fa Flow Boiling inside a 4.2 mm ID Microfin Tube. J Phys Conf Ser;923:012016. https://doi.org/10.1088/1742-6596/923/1/012016.

Longo GA, Mancin S, Righetti G, Zilio C, Doretti L. 2017b. Saturated R134a flow boiling inside a 4.3 mm inner diameter microfin tube. Sci Technol Built Environ;23:933–45. https://doi.org/10.1080/23744731.2017.1300012.

Longo GA, Mancin S, Righetti G, Zilio C. 2019. R1224yd(Z) flow boiling inside a mini microfin tube. *Proc. 25th IIR Int. Congr. Refrig.*, Montréal, Canada https://doi.org/10.18462/iir.icr.2019.0404.

Mancin S, Diani A, Rossetto L. 2014. R134a flow boiling heat transfer and pressure drop inside a 3.4 mm ID microfin tube. Energy Procedia;45:608–15. https://doi.org/10.1016/j.egypro.2014.01.065.

Manwell, S.P., and Bergles, A.E. 1990. Gas-liquid flow patterns in refrigerant-oil mixtures. *ASHRAE Transactions* 96(2):456-464.

Mehendale S. 2017. A new heat transfer coefficient correlation for pure refrigerants and near-azeotropic refrigerant mixtures flow boiling within horizontal microfin tubes. Int J Refrig, 2018;86:292–311. https://doi.org/10.1016/j.ijrefrig.2017.11.017.

Montreal Protocol. 1987. *Montreal Protocol on Substances that Deplete the Ozone Layer*. United Nations (UN), New York, NY, USA (1987 with subsequent amendments).

Ono T, Gao L, Honda T. 2010. Heat transfer and flow characteristics of flow boiling of CO2-oil mixtures in horizontal smooth and micro-fin tubes. Heat Transf Res;39.

Padovan A, Del Col D, Rossetto L. 2011. Experimental study on flow boiling of R134a and R410A in a horizontal microfin tube at high saturation temperatures. Appl Therm Eng;31:3814–26. https://doi.org/10.1016/j.applthermaleng.2011.07.026.

Righetti G, Longo GA, Zilio C, Akasaka R, Mancin S. 2018. R1233zd(E) flow boiling inside a 4.3 mm ID microfin tube. Int J Refrig;91:69–79. https://doi.org/10.1016/j.ijrefrig.2018.04.020.

Righetti G, Longo GA, Zilio C, Mancin S. 2019. Flow boiling of environmentally friendly refrigerants inside a compact enhanced tube. Int J Refrig;104:344–55. https://doi.org/10.1016/j.ijrefrig.2019.05.036.

Schael A-E, Kind M. 2005. Flow pattern and heat transfer characteristics during flow boiling of CO2 in a horizontal micro fin tube and comparison with smooth tube data. Int J Refrig;28:1186–95. https://doi.org/10.1016/j.ijrefrig.2005.09.002.

Schlager, L. M., Pate, M. B., Bergles, A.E. 1990. Evaporation and condensation heat transfer and pressure drop in horizontal, 12.7-mm microfin tubes with refrigerant 22. J Heat Transfer,112:1041–7. https://doi.org/10.1115/1.2910476.

Tang W, Li W. 2018. A new heat transfer model for flow boiling of refrigerants in micro-fin tubes. Int J Heat Mass Transf 2018;126:1067–78. https://doi.org/10.1016/j.ijheatmasstransfer.2018.06.066.

Thome, J. R. 1996. Boiling of new refrigerants: a state-of-the-art review. Int J Refrig, 19:435–57. https://doi.org/10.1016/S0140-7007(96)00004-7.

Thome JR, Favrat D, and Kattan N. 1997. Evaporation in microfin tubes: A generalized prediction model. Proc. Convect. Flow Pool Boil. Conf., Irsee, Germany: 1997.

Webb, R. L., and Kim, N-H. 2005. *Principles of Enhanced Heat Transfer*, 2nd ed., Taylor & Francis, New York.

Wilson, E.E. 1915. A Basis for Rational Design of Heat Transfer Apparatus, Trans. ASME, 37, 47-70.

Wongsa-Ngam J, Nualboonrueng T, Wongwises S. 2004. Performance of smooth and micro-fin tubes in high mass flux region of R-134a during evaporation. Heat Mass Transf Und Stoffuebertragung;40:425–35. https://doi.org/10.1007/s00231-002-0397-5.

Yang C. M., and Hrnjak P. 2019. Effect of helical micro-fins on two-phase flow behavior of R410A evaporating in horizontal round tubes obtained through visualization. Int J Heat Mass Trans, 144:118654. https://doi.org/10.1016/j.ijheatmasstransfer.2019.118654.

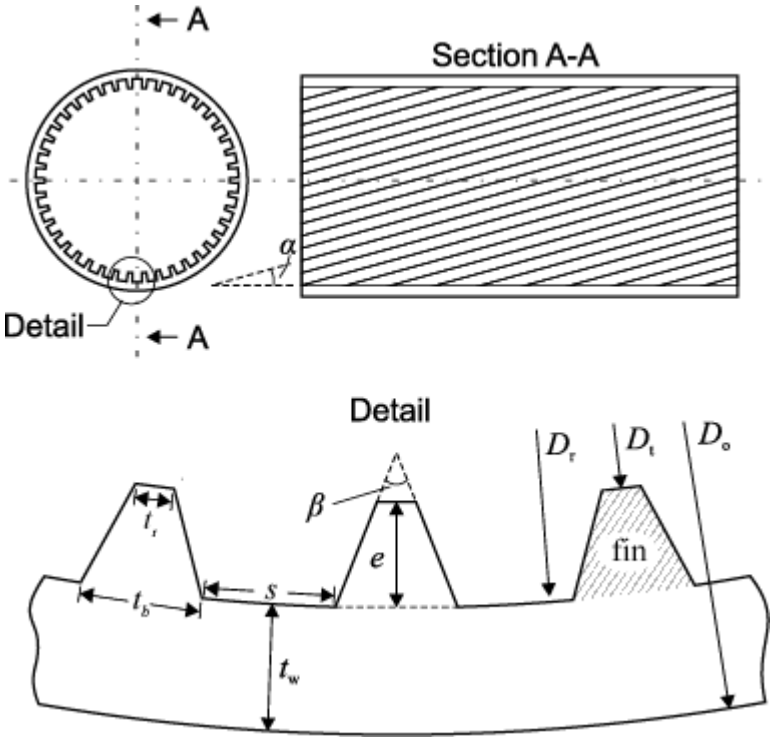

Figure 1 Cross section of a micro-fin tube

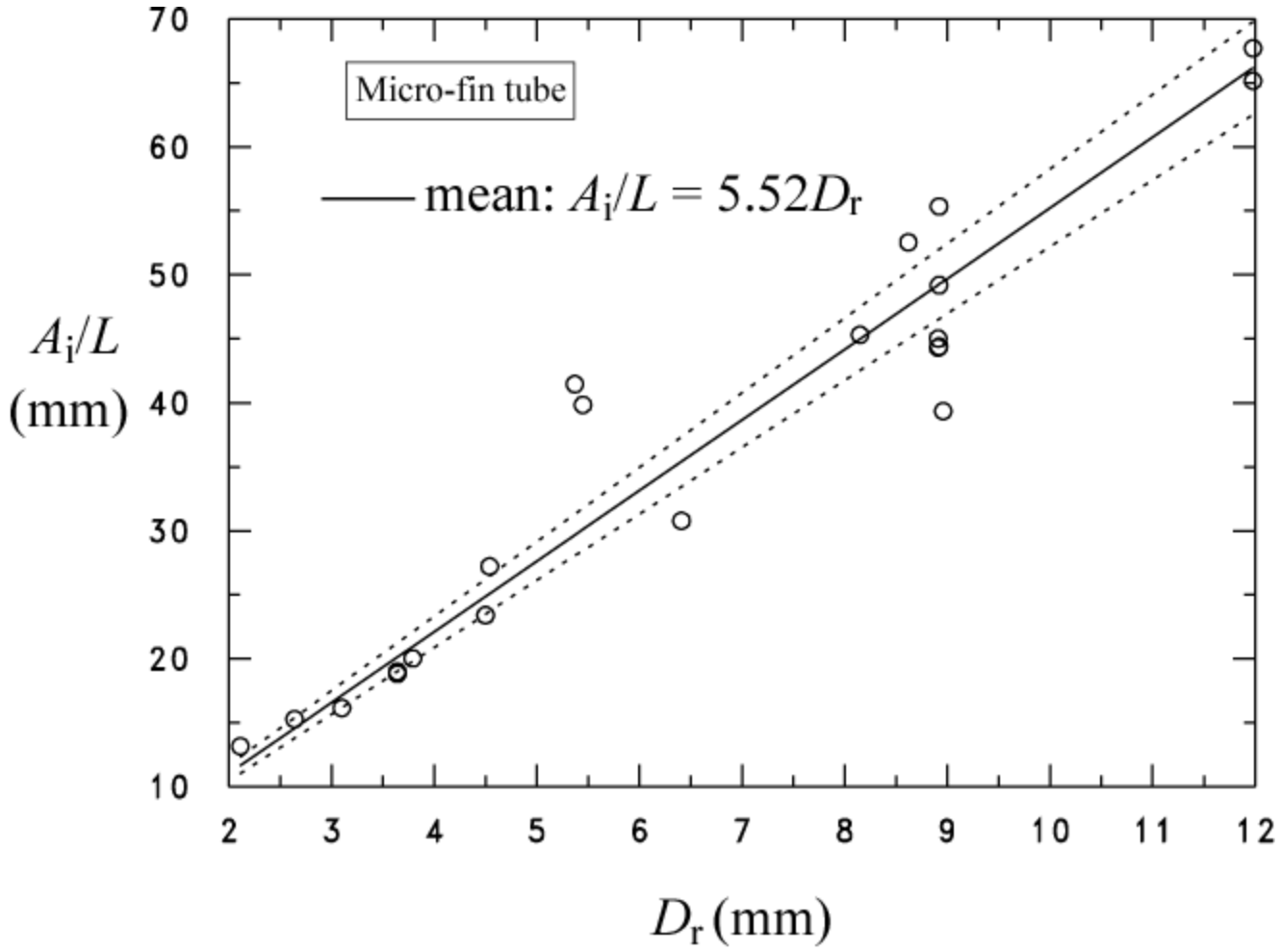

Figure 2 Approximation of the wetted surface area of a micro-fin tube based on the root diameter

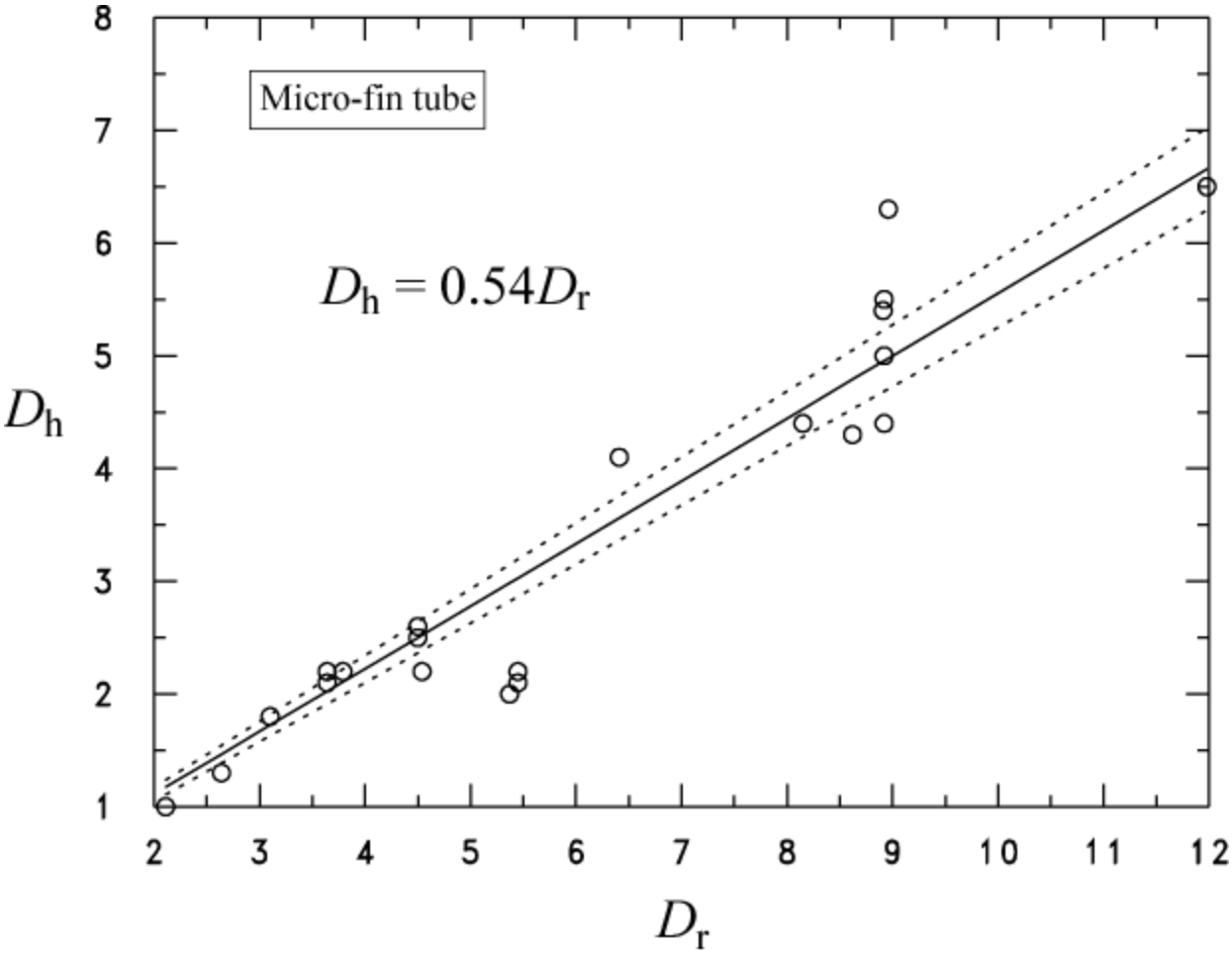

Figure 3 Approximation of the hydraulic diameter based on the root diameter

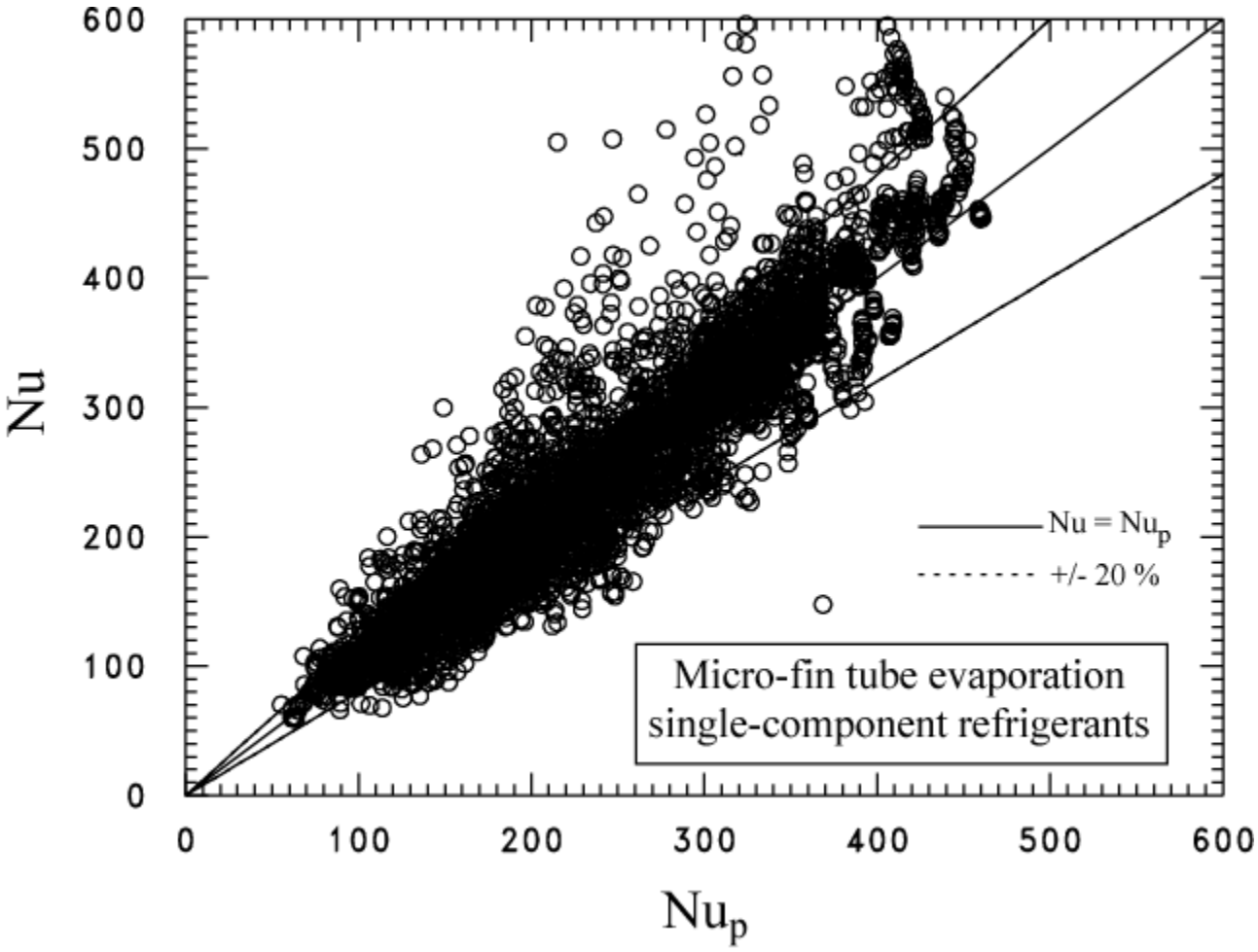

Figure 4 Comparison of measured Nusselt numbers and those predicted by eq (7)

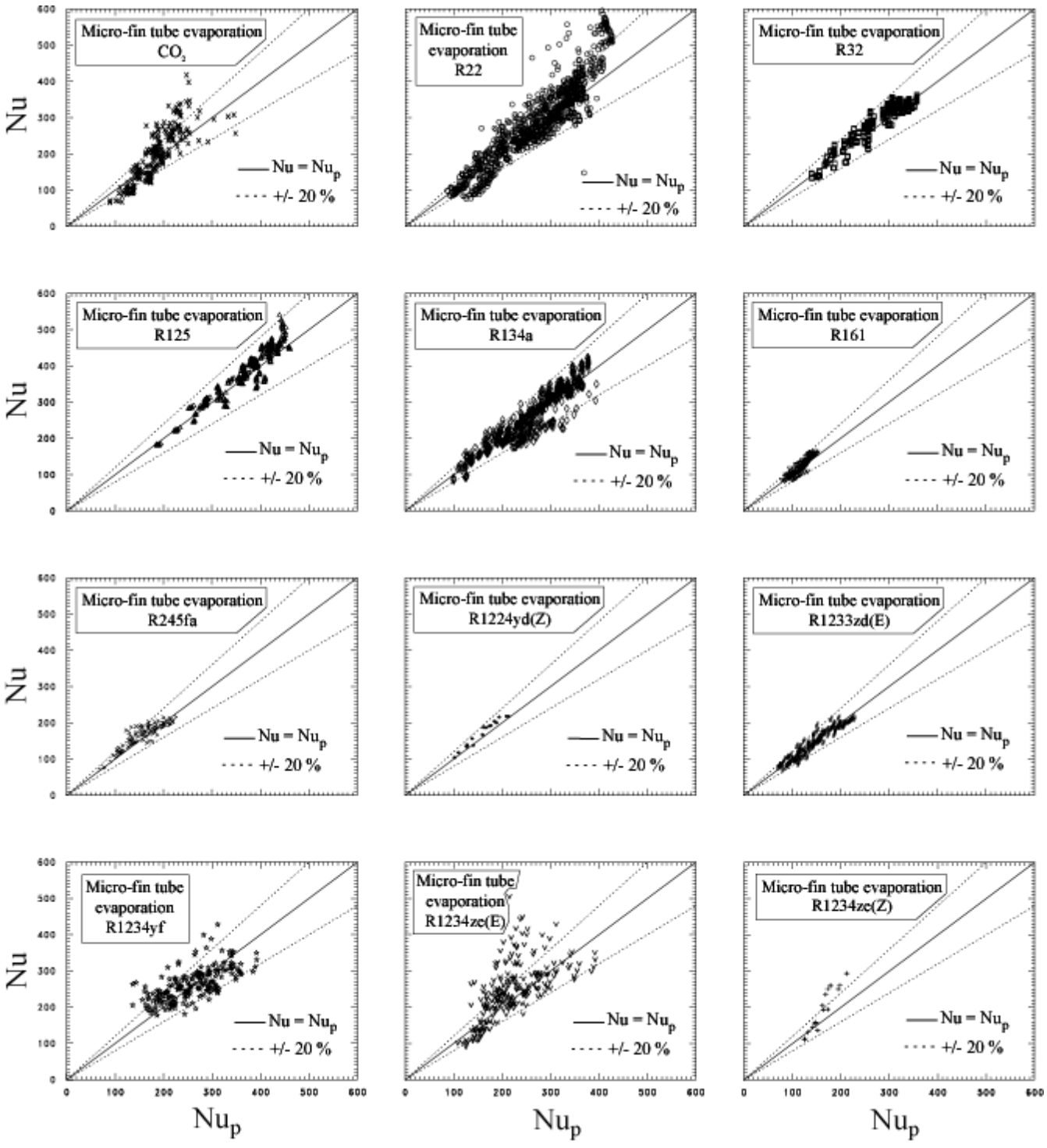

Figure 5 Comparison of measured Nusselt numbers and those predicted by eq. (7) for pure refrigerants

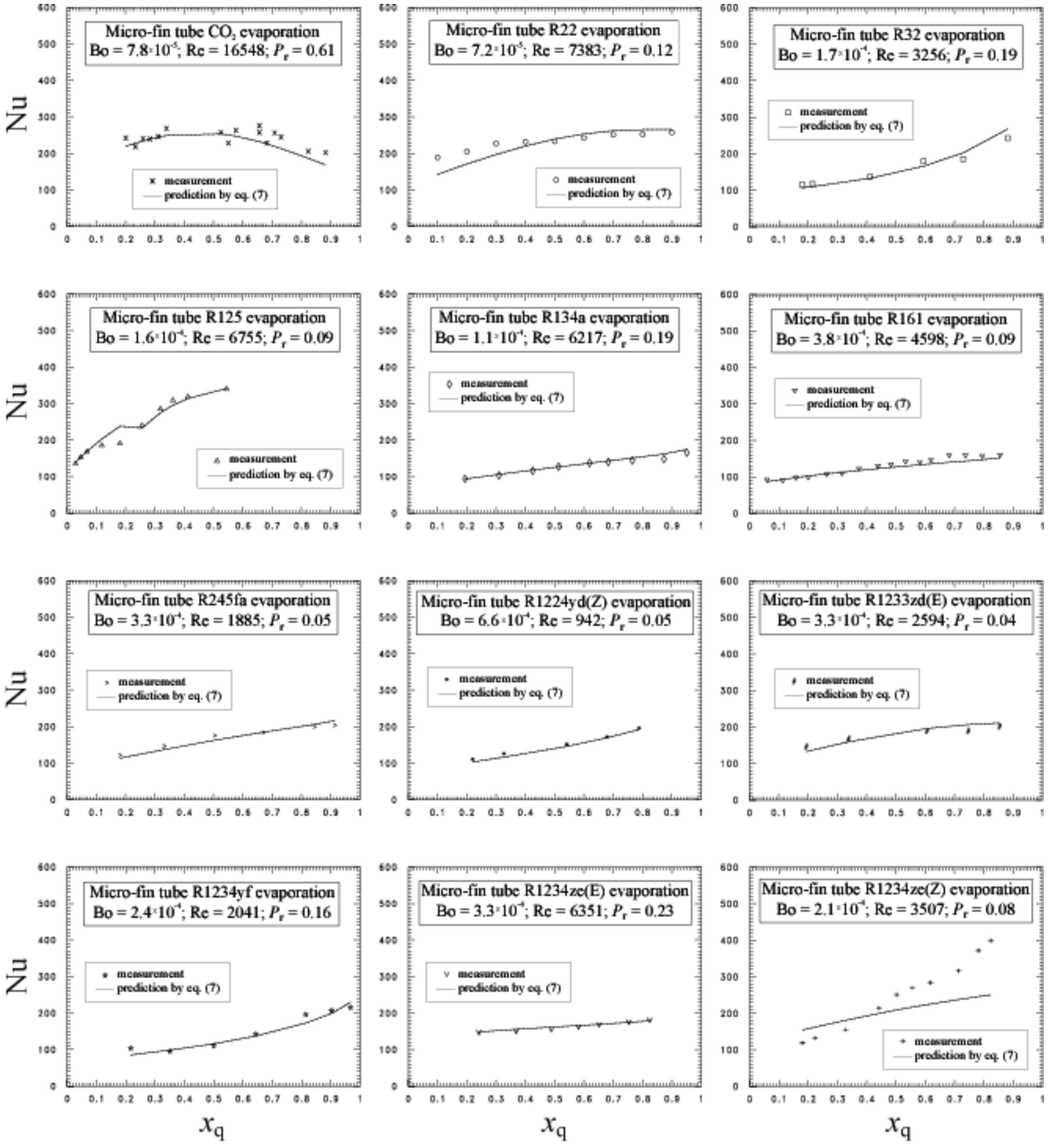

Figure 6 Selected comparison of measured Nusselt numbers and those predicted by eq. (7) for each pure fluid versus quality

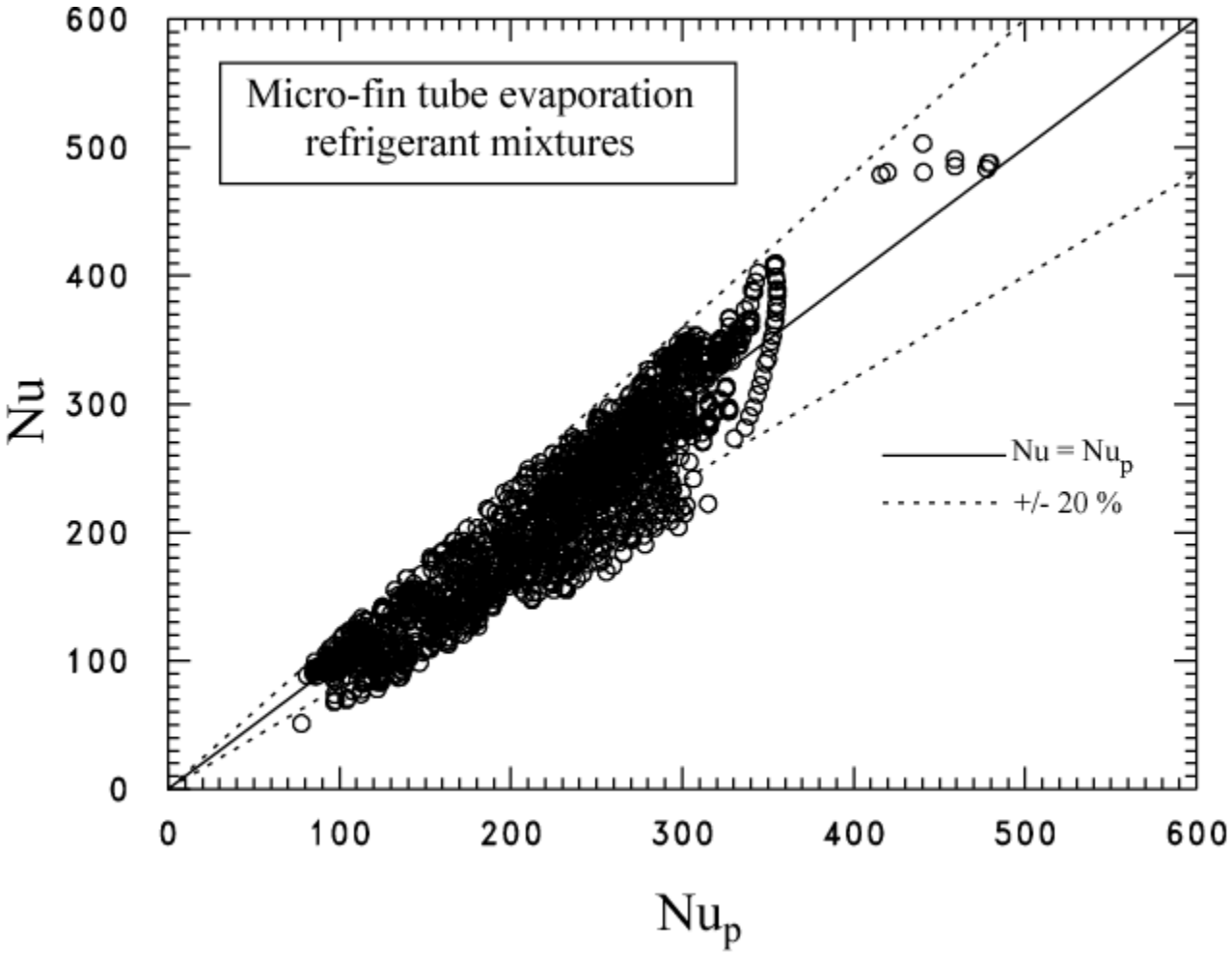

Figure 7 Comparison of measured Nusselt numbers and those predicted by eq. (8)

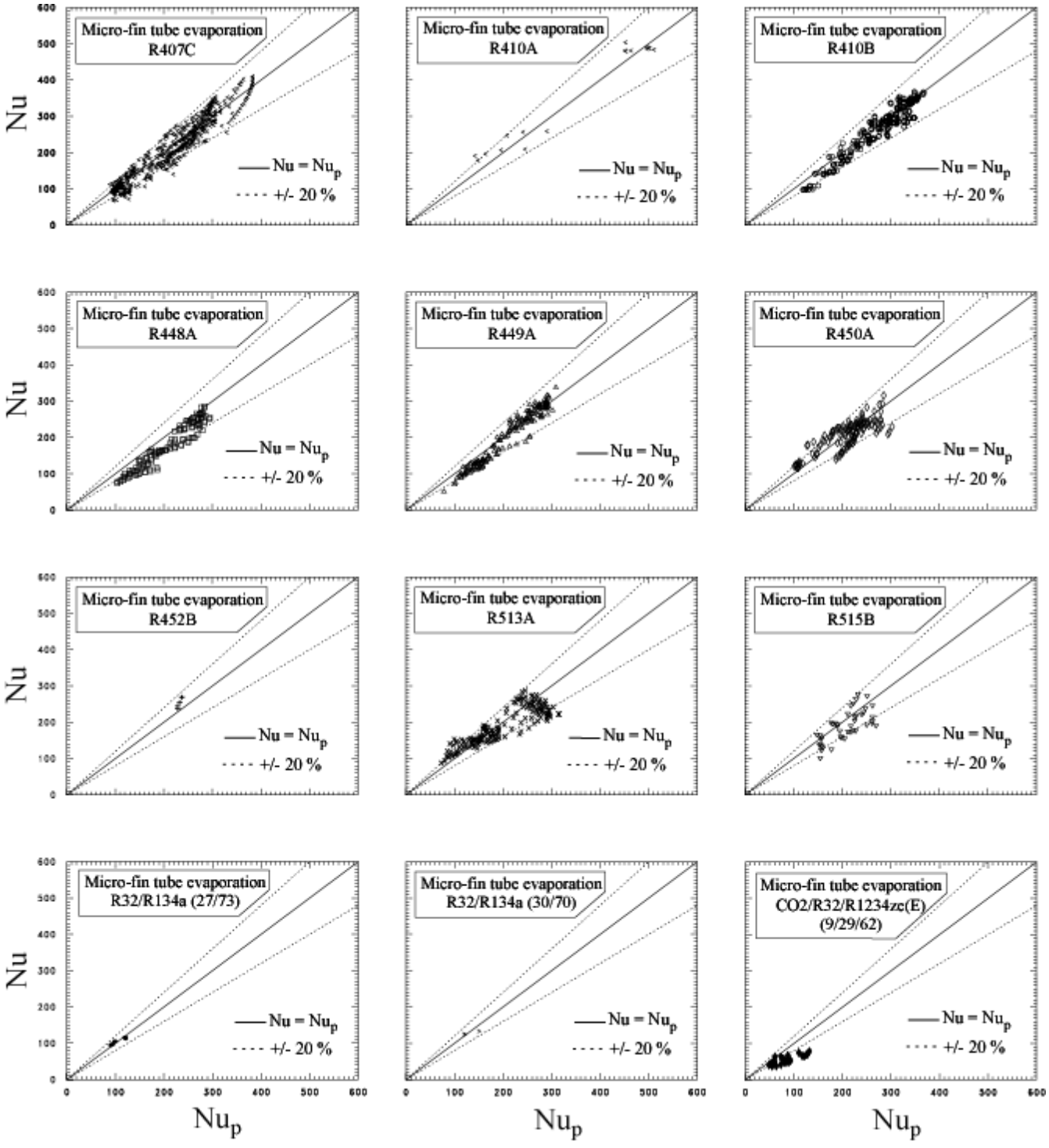

Figure 8 Comparison of measured Nusselt numbers and those predicted by eq. (8) for zeotropic mixtures

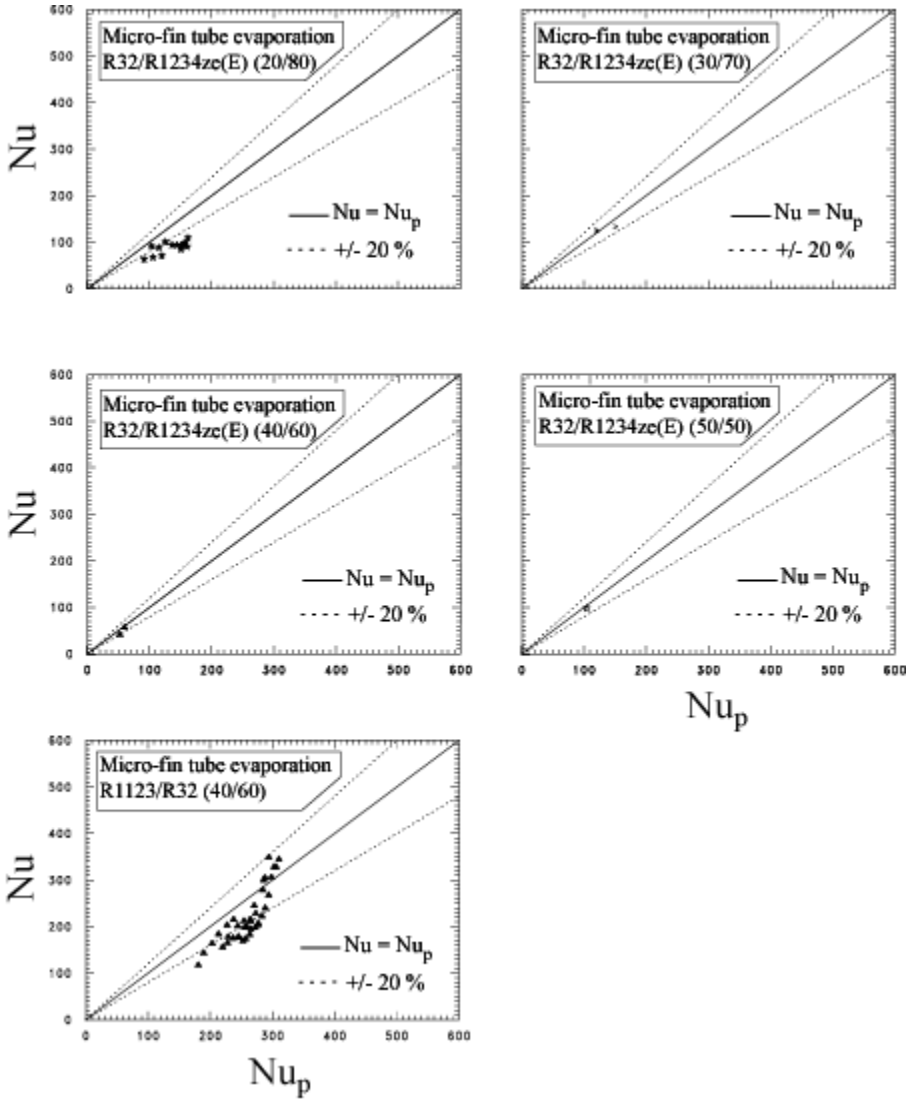

Figure 8(cont) Comparison of measured Nusselt numbers and those predicted by eq. (8) for zeotropic mixtures

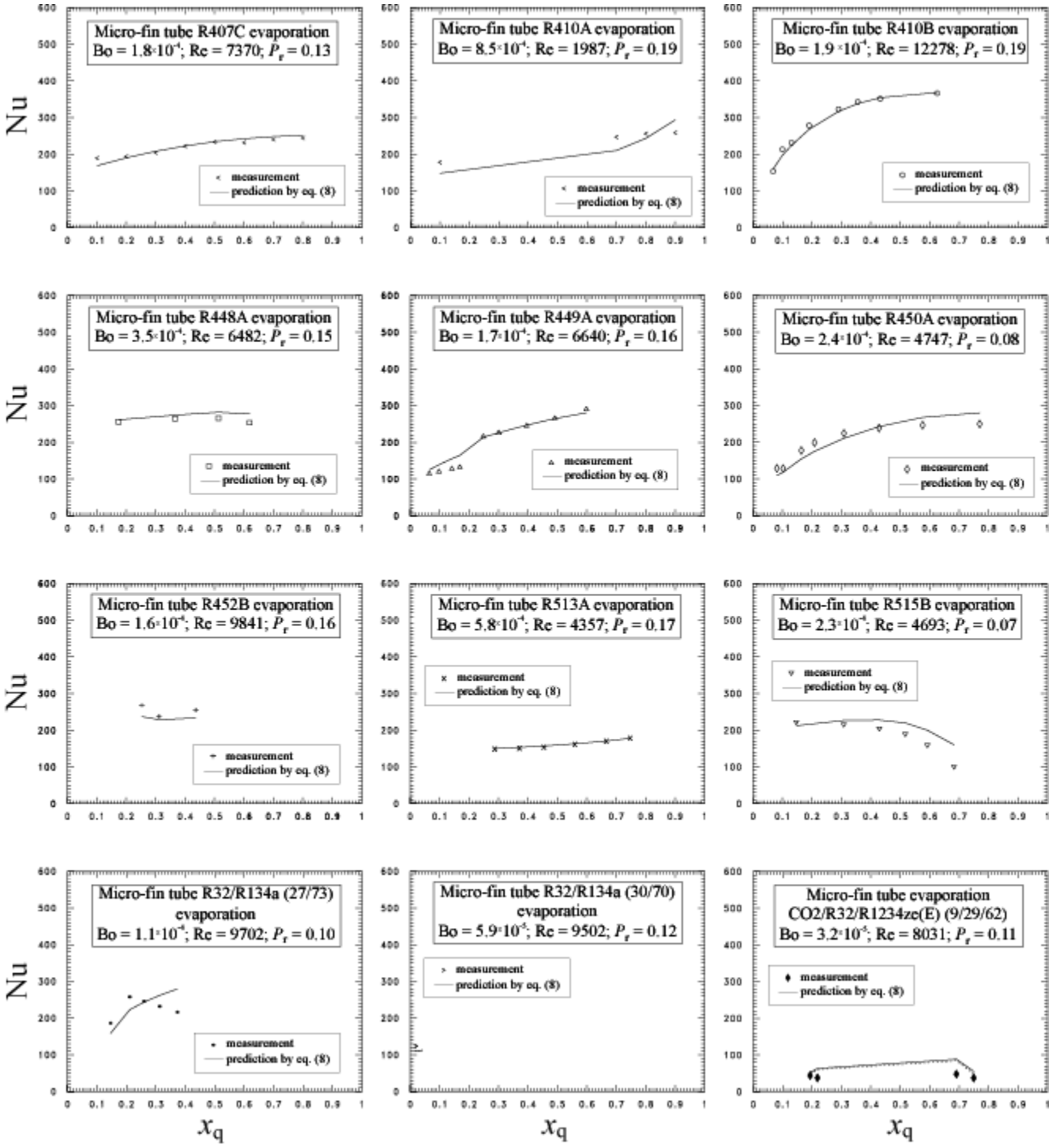

Figure 9 Selected comparison of measured Nusselt numbers and those predicted by eq. (8) for each zeotropic mixture versus quality

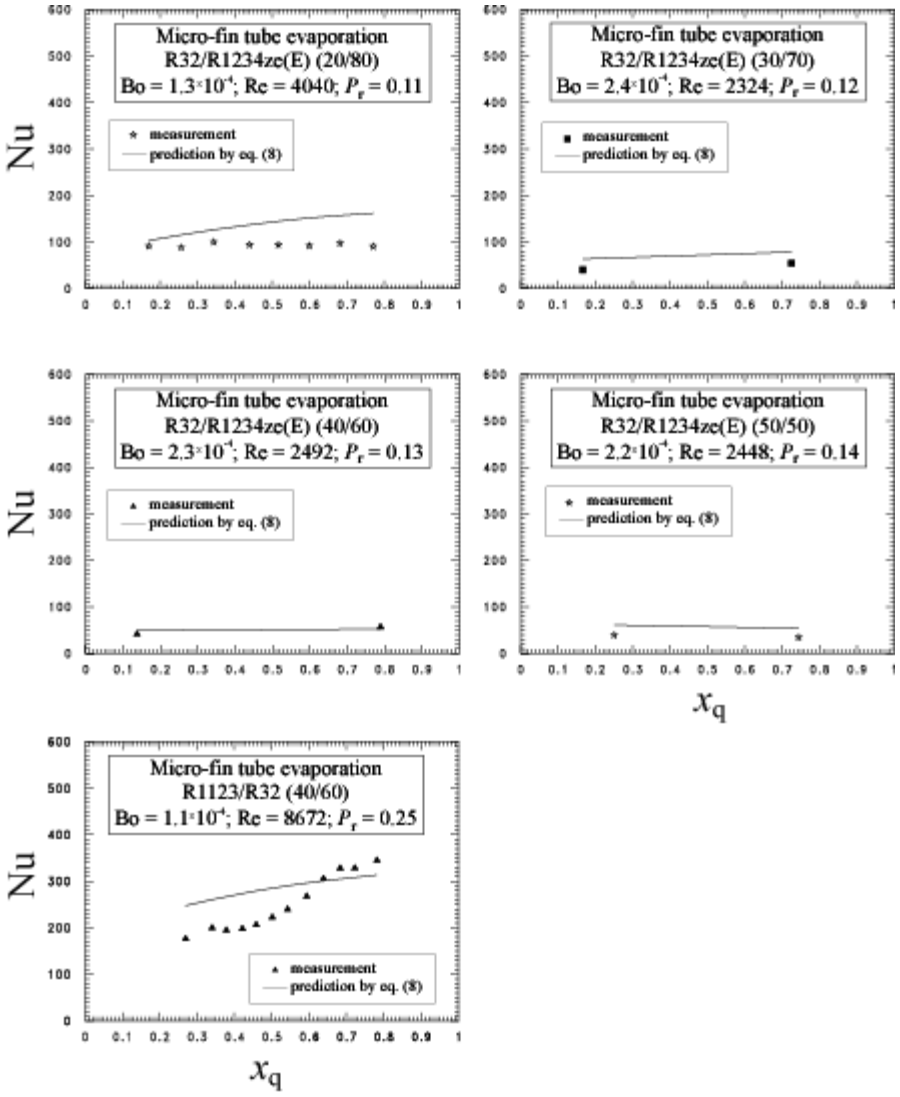

Figure 9(cont) Selected comparison of measured Nusselt numbers and those predicted by eq. (8) for each zeotropic mixture versus quality

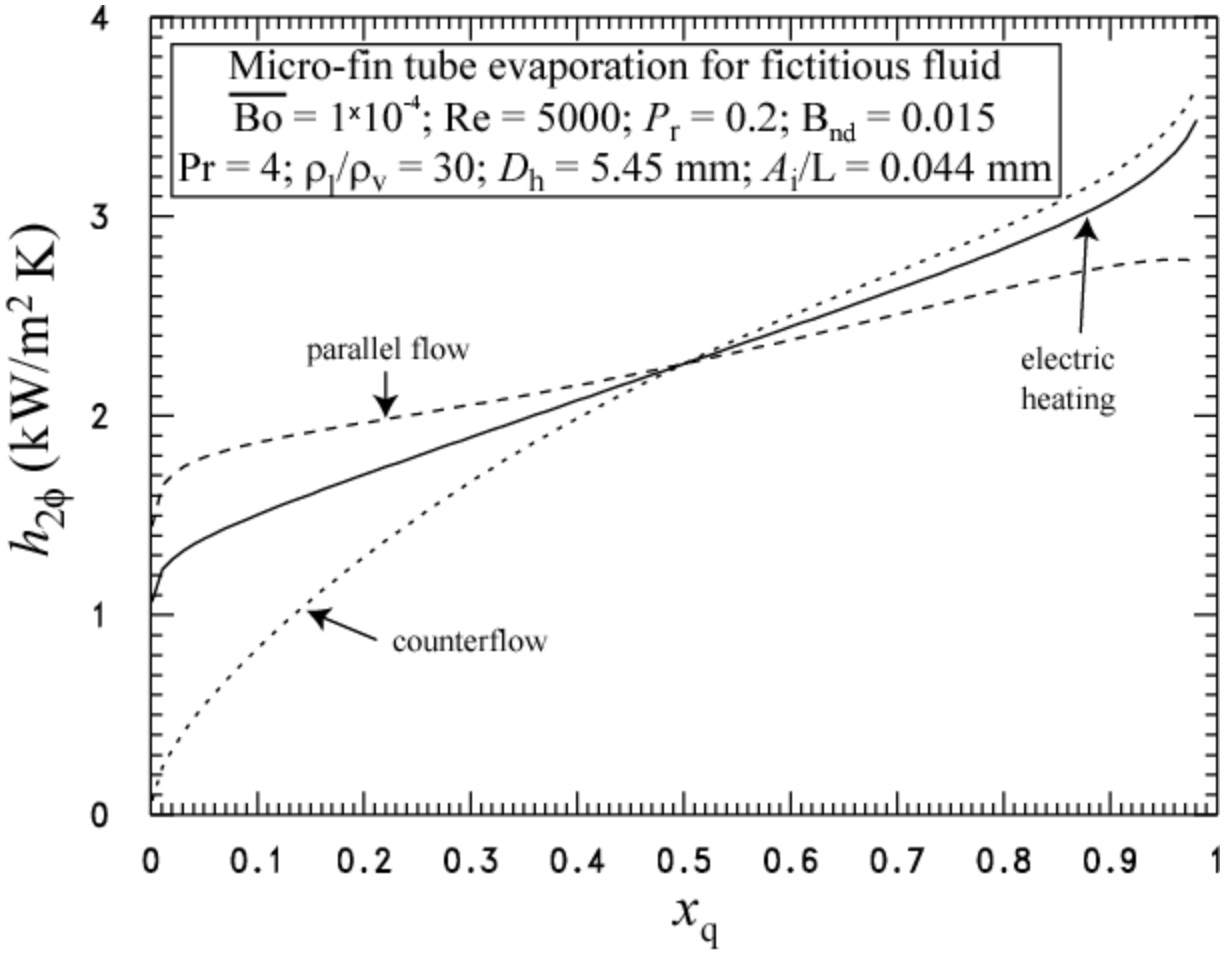

Figure 10 Correlation example for fictitious fluid and three different heating boundary conditions

Table 1 Summary of micro-fin tube operating conditions for database

Source	Fluid	x_q [-]	q'' [kW/m^2]	G [kg/m^{2}s]	T_s [°C]	Heating	Type†	Aq ‡	AG ‡	Ah ‡	L [m]
Lallemand et al. (2001)	R22	0.08 – 0.81	6 – 17	102 – 256	~14	Electric	loc	A_r	A_{cr}	A_r	2.00
Wongsa-Ngam et al. (2004)	R134a	0.16 – 0.89	~6	400 – 800	10 – 15	Electric	avg	A_r	A_{ca}	A_r	2.50
Schael and Kind (2005)	CO_2	0.10 – 0.96	2 – 30	75 – 500	~5	Electric	loc	A_e	A_{ca}	A_e	0.20
Bandarra Filho and Jabardo (2006)	R134a	0.06 – 0.86	~3	102 – 510	~5	Electric	avg	A_r	A_{cr}	A_r	1.50
Gao et al. (2007)	CO_2	0.16 – 0.99	6 – 18	190 – 770	~10	Electric	loc	A_e	A_{ca}	A_e	0.90
Hamilton et al. (2008)	R410B, R134a, R125, R32, R22	0.01 – 0.79	5 – 44	197 – 592	3 – 9	Fluid	loc	A_i	A_{ca}	A_i	6.68
Hu et al. (2008)	R410A					Electric					
Dang et al. (2010)	CO_2	0.12 – 0.97	2 – 8	347 – 693	~15	Electric	loc	A_m	A_{cm}	A_m	1.43
Ono et al. (2010)	CO_2	0.24 – 0.98	6 – 18	190 – 380	~10	Electric	loc	A_e	A_{ca}	A_e	0.90
Bandarra Filho and Barbieri (2011)	R134a	0.06 – 0.92	~3	101 – 506	~5	Electric	avg	A_r	A_{cr}	A_r	1.50
Padovan et al. (2011)	R410A, R134a	0.13 – 0.95	8 – 23	74 – 557	30 – 31	Fluid	avg	A_t	A_{ct}	A_t	0.30
Baba et al. (2012)	R32, R1234ze(E)	0.15 – 0.92	10 – 15	150 – 400	~10	Fluid	avg/seg	A_a	A_{ca}	A_a	0.55
Han et al. (2013a)	R22, R161	0.06 – 0.86	18 – 32	100 – 250	-5 – 8	Electric	loc	A_e	A_{ca}	A_e	2.00
Han et al. (2013b)	R1234yf	0.23 – 0.79	3 – 8	100 – 400	5 – 15	Electric	loc	A_e	A_{ca}	A_e	2.00
Kedzierski and Park (2013)	R134a, R513A, R1234ze(E)	0.01 – 0.82	5 – 42	100 – 418	2 – 13	Fluid	loc	A_i	A_{ca}	A_i	6.68
Kondou et al. (2013)	R1234ze(E)	0.17 – 0.77	~10	191 – 352	~10	Fluid	avg/seg	A_i	A_{ca}	A_i	0.41
Kondou et al. (2014a)	R1234ze(Z), R134a, R1234ze(E)	0.20 – 0.98	~10	150 – 300	~30	Fluid	avg/seg	A_i	A_{ca}	A_i	0.41
Kondou et al. (2014b)	R32, R1234ze(E)	0.06 – 0.78	~10	~200	~10	Fluid	avg/seg	A_i	A_{ca}	A_i	0.41
Diani et al. (2014)	R1234ze(E)	0.18 – 0.88	7 – 33	174 – 859	~30	Electric	avg	A_o	A_{ct}	A_t	0.30
Mancin et al. (2014)	R134a	0.20 – 0.98	7 – 33	174 – 690	~30	Electric	avg	A_o	A_{ct}	A_t	0.30
Diani et al. (2015)	R1234yf	0.19 – 0.97	7 – 33	174 – 859	~30	Electric	avg	A_o	A_{ct}	A_t	0.30
Diani and Rossetto (2015)	R1234yf, R134a	0.19 – 0.98	6 – 32	339 – 683	~30	Electric	avg	A_o	A_{ct}	A_t	0.23
Kedzierski and Kang (2016)	R448A, R449A, R452B	0.04 – 0.87	5 – 19	96 – 318	0 – 9	Fluid	loc	A_i	A_{ca}	A_i	6.68
Diani et al. (2016)	R1234ze(E)	0.16 – 0.99	6 – 32	339 – 850	~30	Electric	avg	A_o	A_{ct}	A_t	0.23
Jiang et al. (2016)	R410A, R134a, R22	0.10 – 0.90	3 – 14	48 – 430	~5	Fluid	avg	A_t	A_{ct}	A_t	1.00
Longo et al. (2017a)	R245fa	0.18 – 0.91	~17	94 – 282	30 – 60	Electric	avg	A_t	A_{ct}	A_t	0.20
Longo et al. (2017b)	R134a	0.07 – 0.96	7 – 42	91 – 729	~30	Electric	avg	A_t	A_{ct}	A_t	0.20
Diani et al. (2017)	R1234yf	0.20 – 0.98	6 – 32	339 – 850	~30	Electric	avg	A_o	A_{ct}	A_t	0.23
Diani and Rossetto (2018)	R134a	0.19 – 0.98	6 – 32	339 – 850	~30	Electric	avg	A_o	A_{ct}	A_t	0.23
Kedzierski and Kang (2018)	R1234yf, R450A, R134a	0.04 – 0.87	5 – 19	96 – 318	0 – 9	Fluid	loc	A_i	A_{ca}	A_i	6.68
Righetti et al. (2018)	R1233zd(E)	0.27 – 0.88	7 – 42	90 – 271	~30	Electric	loc	A_t	A_{ct}	A_t	0.20
Kondou et al. (2019)	R1123/R32 (40/60)	0.20 – 0.80	~10	~200	~10	Fluid	avg/seg	A_i	A_{ca}	A_i	0.41
Longo et al. (2019)	R1224yd(Z)	0.29 – 0.84	8 – 34	94 – 188	~30	Electric	avg	A_t	A_{ct}	A_t	0.20
Righetti et al. (2019)	R1233zd(E), R245fa	0.12 – 0.95	8 – 50	91 – 272	~30	Electric	avg	A_t	A_{ct}	A_t	0.20
Diani and Rossetto (2019)	R513A	0.13 – 0.96	7 – 34	136 – 723	~20	Electric	avg	A_t	A_{ct}	A_t	0.30
Kedzierski and Lin (2021)	R513A, R515B, R450A	0.04 – 0.87	5 – 19	96 – 318	0 – 9	Fluid	loc	A_i	A_{ca}	A_i	6.68

† Whether the data are evaluated locally (loc), averaged over the test tube (avg), or averaged over each segment of the tube (avg/seg)

‡ *Aq*, *AG*, and *Ah* denote the types of base area for q'', G_r, and $h_{2\phi}$, respectively. Refer to the Nomenclature for the definitions and equations for different types of base area used in the literature.

Table 2 Summary of micro-fin tube geometry parameters for database

Source	Fluid	D_r [mm]	α [°]	β [°]	e [mm]	n_f [-]	t_b* [mm]	t_t* [mm]	D_h [mm]
Lallemand et al. (2001)	R22	11.98	20, 30	40, 50	0.25	65, 70	0.291, 0.227	0.170, 0.189	6.5, 6.7
Wongsa-Ngam et al. (2004)	R134a	8.92	18	54*	0.20	60	0.206	0.049	5.5
Schael and Kind (2005)	CO_2	8.62	18	30	0.25	60	0.167	0.085	4.3
Bandarra Filho and Jabardo (2006)	R134a	8.92	18	33	0.20	82	0.136	0.063	4.4
Gao et al. (2007)	CO_2	3.10	12	40	0.11	40	0.100	0.029	1.8
Hamilton et al. (2008)	R410B, R134a, R125, R32, R22	8.91	18	50	0.20	60	0.207	0.067	5.4
Hu et al. (2008)	R410A	6.50	18	40	0.18	50	0.150	0.100	3.55
Dang et al. (2010)	CO_2	2.11	6	35	0.12	40	0.095	0.000	1.0
Ono et al. (2010)	CO_2	3.79	12	40	0.11	50	0.084	0.016	2.2
Bandarra Filho and Barbieri (2011)	R134a	8.92	18	25*	0.20	60	0.111	0.061	5.0
Padovan et al. (2011)	R410A, R134a	8.15	13	43	0.23	60	0.248	0.090	4.4
Baba et al. (2012)	R32, R1234ze(E)	5.37	19	31*	0.26	58	0.180	0.073	2.0
Han et al. (2013a)	R22, R161	6.41	15	34	0.10	65	0.136	0.096	4.1
Han et al. (2013b)	R1234yf	6.41	15	34	0.10	65	0.136	0.096	4.1
Kedzierski and Park (2013)	R134a, R513A, R1234ze(E)	8.91	18	50	0.20	60	0.291	0.133	5.4
Kondou et al. (2013)	R1234ze(E)	5.45	20	18	0.26	48	0.137	0.088	2.2
Kondou et al. (2014a)	R1234ze(Z), R134a, R1234ze(E)	5.45	20	18	0.26	48	0.137	0.088	2.2
Kondou et al. (2014b)	R32, R1234ze(E)	5.45	20	18	0.26	48	0.137	0.088	2.2
Diani et al. (2014)	R1234ze(E)	3.64	18	43	0.12	40	0.145	0.081	2.1
Mancin et al. (2014)	R134a	3.64	18	43	0.12	40	0.145	0.081	2.1
Diani et al. (2015)	R1234yf	3.64	18	43	0.12	40	0.145	0.081	2.1
Diani and Rossetto (2015)	R1234yf, R134a	2.64	7	43	0.12	40	0.145	0.068	1.3
Kedzierski and Kang (2016)	R448A, R449A, R452B	8.91	18	50	0.20	60	0.207	0.067	5.4
Diani et al. (2016)	R1234ze(E)	2.64	7	43	0.12	40	0.145	0.068	1.3
Jiang et al. (2016)	R410A, R134a, R22	8.96	18	66	0.14	60	0.224	0.108	6.3
Longo et al. (2017a)	R245fa	4.50	18	42	0.15	40	0.256	0.177	2.5
Longo et al. (2017b)	R134a	4.54	27	11	0.12	54	0.154	0.154	2.2
Diani et al. (2017)	R1234yf	2.64	7	43	0.12	40	0.145	0.068	1.3
Diani and Rossetto (2018)	R134a	2.64	7	43	0.12	40	0.145	0.068	1.3
Kedzierski and Kang (2018)	R1234yf, R450A, R134a	8.91	18	50	0.20	60	0.207	0.067	5.4
Righetti et al. (2018)	R1233zd(E)	4.54	27	11	0.12	54	0.154	0.154	2.2
Kondou et al. (2019)	R1123/R32 (40/60)	5.45	20	18	0.26	48	0.137	0.088	2.2
Longo et al. (2019)	R1224yd(Z)	4.50	18	42	0.15	40	0.256	0.177	2.5
Righetti et al. (2019)	R1233zd(E), R245fa	4.50	18	42	0.15	40	0.158	0.079	2.6
Diani and Rossetto (2019)	R513A	3.64	18	43	0.12	40	0.123	0.065	2.1
Kedzierski and Lin (2021)	R513A, R515B, R450A	8.91	18	50	0.20	60	0.207	0.067	5.4

* Estimated from the photo of micro-fins or by matching the given geometric properties such as area enlargement ratio, depending on whichever is available

Table 3 Representative properties from REFPROP (Lemmon et al. 2018)

Test fluid	Evaluated at T_s = 277.6 K									
	$T_d - T_b$ (K)	k_l W m^{-1} K^{-1}	Pr	σ mN m^{-1}	ρ_l (kg m^{-3})	ρ_v (kg m^{-3})	$[P_s]_{xq=0}$ (kPa)	c_p (J kg^{-1}K^{-1})	i_{fg} (kJ kg^{-1})	μ_l (μPa s)
CO_2	0.000	0.104	2.41	3.7	899.6	112.6	3913.9	2703	216.82	92.77
R22	0.000	0.092	2.63	11.1	1265.9	24.4	575.9	1182	201.33	205.53
R32	0.000	0.142	1.79	10.2	1039.3	25.5	938.3	1771	308.04	143.06
R125	0.000	0.068	3.59	6.4	1298.3	48.6	772.2	1275	129.51	190.93
R134a	0.000	0.090	3.78	10.8	1279.6	16.9	344.2	1354	195.09	251.54
R161	0.000	0.124	2.55	12.1	740.0	11.9	504.32	2133	368.92	148.48
R245fa	0.000	0.095	7.23	16.3	1392.6	3.9	64.99	1270	202.42	539.77
R1224yd(Z)	0.000	0.083	4.98	15.2	1416.1	4.5	67.42	1094	173.46	377.34
R1233zd(E)	0.000	0.089	4.71	17.3	1311.1	3.4	58.31	1184	201.46	353.57
R1234yf	0.000	0.070	3.63	8.8	1161.8	20.4	367.5	1306	160.32	194.27
R1234ze(E)	0.000	0.081	4.04	11.7	1226.7	13.7	255.2	1329	181.25	247.48
R1234ze(Z)	0.000	0.091	4.30	15.4	1277.2	4.2	82.12	1219	218.02	319.88
R407C	6.013	0.094	3.04	9.4	1219.4	26.4	656.7	1433	212.50	199.11
R410A	0.110	0.101	2.34	8.2	1151.9	35.2	920.5	1544	215.80	152.90
R410B	0.150	0.097	2.43	8.0	1164.5	35.8	918.0	1521	212.36	155.03
R448A	5.552	0.091	2.83	8.9	1180.7	28.8	717.4	1441	207.93	178.40
R449A	5.153	0.090	2.87	8.7	1180.6	28.8	706.0	1436	205.59	179.28
R450A	0.640	0.084	3.89	11.2	1245.4	15.7	305.0	1339	186.54	245.39
R452B	1.137	0.116	2.05	9.2	1075.8	28.0	884.4	1636	261.49	145.74
R513A	0.015	0.078	3.65	9.5	1206.9	20.1	379.4	1329	172.28	212.68
R515B	0.019	0.080	4.10	11.6	1245.8	14.0	253.5	1310	176.50	251.19
R1123/R32 (40/60)	1.77	0.114	2.06	7.7	1044.5	37.0	1190.3	1755	241.17	133.66
R32/R134a (27/73)	6.262	0.103	2.87	10.4	1194.0	20.9	609.1	1477.	252.82	200.19
R32/R134a (30/70)	6.190	0.102	2.94	10.5	1201.9	20.6	588.1	1465	248.86	204.16
CO2/32/1234ze(E) 9/29/62	21.40	0.106	2.60	10.4	1145.5	18.9	1016.8	1524	233.55	180.14
32/1234ze(E) (20/80)	12.27	0.095	3.01	11.4	1189.3	15.9	545.7	1407	210.04	203.82
32/1234ze(E) (30/70)	11.91	0.102	2.77	11.2	1170.3	17.2	632.0	1449	221.27	194.52
32/1234ze(E) (40/60)	10.42	0.108	2.51	11.1	1151.4	18.6	699.4	1493	232.43	182.46
32/1234ze(E) (50/50)	8.45	0.115	2.31	10.9	1132.4	20.2	754.5	1537	243.82	172.58

Table 4 Parameters range of database

Parameter	Minimum	Maximum
G_r [kg m^{-2}·s^{-1}]	48	859
T_s [K]	268.1	333.1
D_r [mm]	2.11	11.98
D_h [mm]	0.95	6.67
α [°]	6.3	30.0
β [°]	11	66
e [mm]	0.10	0.26
n_f [-]	40	82
q" [kW m^{-2}]	0.7	50.5
Bd	3.5×10^{-3}	3.8×10^{-2}
Bo	1.2×10^{-5}	1.9×10^{-3}
Co	5.7×10^{-3}	20
Nu	38	743
Re	628	23512
$\frac{\rho_l}{\rho_v}$	5	147
Pr	1.77	5.75
P_s/P_c	0.04	0.69
x_q	0.002	0.986
$\frac{T_d - T_b}{T_b}$	6.8×10^{-6}	8.4×10^{-2}

Table 5 Conversions for alternate based to A_{ca} base and D_h base mass velocities and Re

Alternate flow area, alternate diameter	To convert from a mass velocity based on an alternate flow area to one based on the actual flow area, multiply by	To convert from a two-phase Reynolds number based on an alternate diameter to the all-liquid Reynolds number based on D_h, multiply by
A_{cm}, D_m	$\frac{\pi D_m^2}{4A_{ca}}$	$\frac{\pi D_m D_h}{4\left(1-x_q\right)A_{ca}}$
A_{cr}, D_r	$\frac{\pi D_r^2}{4A_{ca}}$	$\frac{\pi D_r D_h}{4\left(1-x_q\right)A_{ca}}$
A_{ct}, D_t	$\frac{\pi D_t^2}{4A_{ca}}$	$\frac{\pi D_t D_h}{4\left(1-x_q\right)A_{ca}}$
A_{co}, D_o	$\frac{\pi D_o^2}{4A_{ca}}$	$\frac{\pi D_o D_h}{4\left(1-x_q\right)A_{ca}}$

Table 6 Conversions for alternate based to A_i base and D_h base q'', $h_{2\phi}$, and Nu

Alternate surface area, alternate diameter	To convert from a heat flux based on an alternate surface area to one based on the actual surface area, multiply by	To convert from a heat transfer coefficient based on an alternate surface area to one based on the actual surface area, multiply by	To convert from a Nusselt number based on an alternate surface area and alternate diameter to one based on the actual surface area and D_h, multiply by
A_e, D_e	$\frac{\pi D_e}{A_i / L}$	$\frac{\pi D_e}{A_i / L}$	$\frac{\pi D_h}{A_i / L}$
A_m, D_m	$\frac{\pi D_m}{A_i / L}$	$\frac{\pi D_m}{A_i / L}$	$\frac{\pi D_h}{A_i / L}$
A_r, D_r	$\frac{\pi D_r}{A_i / L}$	$\frac{\pi D_r}{A_i / L}$	$\frac{\pi D_h}{A_i / L}$
A_t, D_t	$\frac{\pi D_t}{A_i / L}$	$\frac{\pi D_t}{A_i / L}$	$\frac{\pi D_h}{A_i / L}$